Ocean Systems Engineering, *Vol. 6, No. 1 (2016) 61-97*
DOI: http://dx.doi.org/10.12989/ose.2016.6.1.061

Impacts of wave and tidal forcing on 3D nearshore processes on natural beaches. Part II: Sediment transport

R. Bakhtyar*[1], A. Dastgheib[2], D. Roelvink[2,3] and D.A. Barry[4]

[1]*Davidson Laboratory, Stevens Institute of Technology, Hoboken, NJ 07030, USA*
[2]*UNESCO-IHE, PO Box 3015, 2601 DA Delft, The Netherlands*
[3]*Technical University of Delft, PO Box 5048, 2600 GA, Delft, The Netherlands, and Deltares, PO Box 177, 2600 MH, Delft, The Netherlands*
[4]*Laboratoire de technologie écologique, Institut d'ingénierie de l'environnement, Faculté de l'environnement naturel, architectural et construit (ENAC), Station 2, Ecole polytechnique fédérale de Lausanne (EPFL), 1015 Lausanne, Switzerland*

(Received July 1, 2015, Revised February 2, 2016, Accepted February 9, 2016)

Abstract. This is the second of two papers on the 3D numerical modeling of nearshore hydro- and morphodynamics. In Part I, the focus was on surf and swash zone hydrodynamics in the cross-shore and longshore directions. Here, we consider nearshore processes with an emphasis on the effects of oceanic forcing and beach characteristics on sediment transport in the cross- and longshore directions, as well as on foreshore bathymetry changes. The Delft3D and XBeach models were used with four turbulence closures (viz., *k*-ε, *k*-*L*, ATM and H-LES) to solve the 3D Navier-Stokes equations for incompressible flow as well as the beach morphology. The sediment transport module simulates both bed load and suspended load transport of non-cohesive sediments. Twenty sets of numerical experiments combining nine control parameters under a range of bed characteristics and incident wave and tidal conditions were simulated. For each case, the general morphological response in shore-normal and shore-parallel directions was presented. Numerical results showed that the *k*-ε and H-LES closure models yield similar results that are in better agreement with existing morphodynamic observations than the results of the other turbulence models. The simulations showed that wave forcing drives a sediment circulation pattern that results in bar and berm formation. However, together with wave forcing, tides modulate the predicted nearshore sediment dynamics. The combination of tides and wave action has a notable effect on longshore suspended sediment transport fluxes, relative to wave action alone. The model's ability to predict sediment transport under propagation of obliquely incident wave conditions underscores its potential for understanding the evolution of beach morphology at field scale. For example, the results of the model confirmed that the wave characteristics have a considerable effect on the cumulative erosion/deposition, cross-shore distribution of longshore sediment transport and transport rate across and along the beach face. In addition, for the same type of oceanic forcing, the beach morphology exhibits different erosive characteristics depending on grain size (e.g., foreshore profile evolution is erosive or accretive on fine or coarse sand beaches, respectively). Decreasing wave height increases the proportion of onshore to offshore fluxes, almost reaching a neutral net balance. The sediment movement increases with wave height, which is the dominant factor controlling the beach face shape.

Keywords: beach profile changes; longshore sediment transport; bed load; suspended load; on/offshore sediment transport

1. Introduction

*Corresponding author, E-mail: roham.bakhtyar@stevens.edu

http://www.techno-press.org/?journal=ose&subpage=7 ISSN: 2093-6702 (Print), 2093-677X (Online)

Effective and economical design of beach protection schemes need to account for sediment-flow interactions in the surf and swash zones, in particular the simulation of such interactions in 3D (Elfrink and Baldock 2002, Polome *et al*. 2005, Roelvink and Reniers 2012). Oceanic forcing in the nearshore zone produces sediment transport in both cross- and longshore directions, and thereby induces foreshore profile changes (Longuet-Higgins 1970, Chen *et al*. 2003, Johnson and Smith 2005). When waves propagate obliquely towards the shore, longshore currents occur, as well as cross-shore and return flows (Celikoglu *et al*. 2004). The wave-current interactions are important as they affect nearshore circulation, as well as sediment transport (Feddersen *et al*. 1998, Garcez Faria *et al*. 1998, Reniers *et al*. 2004, 2009, Newberger and Allen 2007a,b).

Both longshore and cross-shore sediment transport control beach morphology (Kamphuis 1991, Kumar *et al*. 2003, Lee *et al*. 2007, Garnier *et al*. 2008). Numerical process-based morphological models have been used more extensively in 1D, 2DV and 2DH modes, but with increasing computational capacities and acceleration techniques currently 3D numerical models have the potential to simulate the nearshore zone more realistically (Liang *et al*. 2007). Reliable quantitative analyses of the morphodynamic processes taking place in the nearshore zone, including the rates, fluxes and directions of sediment transport, have yet to be fully developed (Masselink and Puleo 2006). Only a few numerical studies have been conducted, most of which used relatively strong simplifying assumptions. In particular, they ignored the impact of longshore currents on sediment transport, although such currents can have strong effects on beach morphology (Elfrink and Baldock 2002, Masselink and Puleo 2006, Bakhtyar *et al*. 2009a, Razmi *et al*. 2011). Notwithstanding that some of the existing models include the swash zone (van Wellen *et al*. 2000), in most Longshore Sediment Transport (LST) models, the swash transport contribution is either completely ignored or merely accounted for as part of the total sediment transport budget. In addition, most studies are based on empirical relations in the surf zone.

Recently, Antuono *et al*. (2007) investigated the integral properties of the swash zone and found that two main terms contribute to the longshore current velocity: (i) short-wave interactions and non-breaking wave nonlinearities, and (ii) momentum transfer due to wave breaking. Baba and Camenen (2008) implemented a LST model for the swash zone in a beach evolution model and found that sediment transport in the swash zone has an important effect on beach profile changes. Because of complex flow processes involved in sediment transport, most of the existing sediment transport models consider cross-shore and longshore processes individually and are thereby limited in predicting LST (Ellis and Stone 2006, Esteves *et al*. 2009). In addition, existing empirical models are often derived from steady flow conditions (Elfrink and Baldock 2002). They are not necessarily applicable to oscillatory flow, such as found in the swash and surf zones, and combined flows (where both waves and currents are significant) (Warner *et al*. 2008). Despite much research on this topic, less attention has been paid to numerical modeling of LST, which is subject to dynamic effects of vortices and turbulence under breaking waves, for example (Bakhtyar *et al*. 2009b). Comprehensive 3D numerical models provide a means to investigate the effects of aforementioned factors on the foreshore morphodynamics, and to provide guidance for the understanding of the nearshore zone processes.

Due to the complexity and uncertainty of flow velocity and sediment dynamics, there is an extensive range of available models (Hanson *et al.* 2003). Three approaches have been used to investigate the morphodynamics of coastal systems driven by sea-level oscillations: (i) behavior-oriented models (Reeve and Fleming 1997, Hanson *et al*. 2003); (ii) two-phase flow

modeling (Drake and Calantoni 2001, Bakhtyar *et al*. 2009b, e, 2010a, 2013c); and (iii) process-based models (Karambas 2006, Pedrozo-Acuna *et al*. 2007, Dastgheib *et al*. 2008, Bakhtyar *et al*. 2009c, 2011, Roelvink *et al*. 2009).

Behavior-oriented models reproduce the behavior of bed morphology using governing equations that are simplified to preserve only the main processes (Reeve and Fleming 1997). Hanson *et al*. (2003) presented models describing coastal evolution on yearly to decadal time scales and suggested that forthcoming efforts should be focused on model integration rather than improvement of individual model concepts. Eulerian two-phase flow models treat separately the sediment and fluid phases. Bakhtyar *et al*. (2010a) investigated the performance of 2D two-phase flow models based on Navier-Stocks (NS) equations, a turbulence closure model and the Volume-Of-Fluid approach. Although the model is relevant to understanding morphology in the surf and swash zones, it is not applicable to 3D field applications. Process-based numerical models (such as Delft3D) simulate major processes in the nearshore zone combining hydrodynamic, sediment transport and foreshore evolution models. Roelvink *et al.* (2009) used a process-based model to assess the coastal response under storm and hurricane circumstances, including dune erosion and breaching, and showed the potential of such a modeling strategy in a number of analytical, laboratory and field cases.

Delft3D is a widely used tool for simulating field-scale coastal engineering problems. Delft3D-Flow has been verified in several practical test cases of 3D modeling of hydrodynamics and sediment transport (Lesser *et al.* 2004, Harcourt-Baldwin and Diedericks 2006, Morelissen *et al*. 2010, van Rijn 2011). It was used in Part I, which described a 3D process-based model for simulating wave and tidal motions on an impermeable beach. Nearshore hydrodynamic behavior through the two-way coupling of hydrodynamic and morphodynamic 3D models (Delft3D and XBeach) were computed and analyzed. The model and the setup used to represent the nearshore area were validated using field data. Good agreement was found considering different conditions, in particular water level elevations, wave height and properties of longshore flows. The main purpose of the present paper is to investigate and describe the sediment transport processes and beach profile changes in the nearshore zone using that model and setup. The same numerical experiments as in Part I are exploited, covering a range of oceanic conditions and beach characteristics. The specific objectives of this study are to:

- Use the model to evaluate the importance of wave characteristics, sediment grain size, beach shape, bed slope and oceanic forcing on 3D beach profile changes in a field setup, and to consider the results in the light of the existing understanding of beach evolution;
- Simulate the effect of longshore flows on the sediment transport and beach morphology;
- Evaluate the feasibility of field-scale sediment transport modeling under mixed and variable conditions of oceanic forcing;
- Examine the overall on/offshore and cross-shore/longshore sediment circulation and dynamics.

2. Methodology

2.1 Model description

In this study, the effect of oceanic forcing on the nearshore morphodynamics was simulated. The three processes (i.e., wave motions, tide motions and sediment movements) were coupled using a sequential approach. Our approach was based on Delft3D (for simulating hydrodynamic

and morphodynamic processes) and XBeach* (for generating wave motion) models. The Delft3D uses a finite difference-method to solve the governing equations on a curvilinear grid, and includes a flooding and drying technique. XBeach resolves wave motion containing waveshoaling, wave refraction, wave breaking and current refraction. We simulated wave and tidal motions in the nearshore area, and flow based on the 3D NS equations and different turbulence closure models (viz., *k*-ε, *k*-*L*, ATM and H-LES). The Delft3D (Delft3D-FLOW: User manual, 2009) sediment transport and beach evolution modules were used to simulate foreshore profile changes. The hydrodynamic model was run to produce the 3D hydrodynamic characteristics. These results and those of XBeach were used as input to calculate the sediment transport and morphology changes. Changes in bed morphology were fed back into the hydrodynamics.

Kinematic boundary conditions were used at the free surface, whereas at the bottom a quadratic bed stress equation was used. Zero normal velocities were applied at the landward boundary. A weakly reflecting boundary condition was used at the open boundaries. Oceanic forcing was generated via postulating the velocity, surface elevation, and wave angle. The driving forces were the incident waves that arrived perpendicular and obliquely or to the beach, and the tide, which propagated from south to north. The seaward boundary was controlled by a time series of water elevations, while lateral boundary conditions (i.e., Neumann boundary condition) were applied as the longshore water level gradient, which corresponds to a progressive wave (Roelvink and Walstra 2004).

Simulations used a non-uniform grid size ranging from 5 m in the nearshore area to 75 m in the offshore region. In all cases, models were run for one month and started from a constant beach face slope. The initial bathymetry of the numerical experiments is alongshore uniform. The final bathymetry is after the one month simulations. After one month, the simulations reach the state that the bed level averaged over a tidal cycle is steady. A detailed description of the model equations, boundary conditions and numerical scheme was given in Delft3D-manual.

2.1.1 Sediment transport and beach morphology models

Both bed load and suspended load transport of non-cohesive sediment were considered in the sediment transport and morphology models. Transport of suspended sediment was calculated using the advection-diffusion equation (van Rijn 2011)

$$\frac{\partial c}{\partial t} + \nabla.\left(\vec{U}'c\right) = \nabla.\left(\varepsilon_d \nabla c\right), \tag{1}$$

where c is the sediment concentration, $\vec{U}' \equiv \left(U, V, w - w_s\right)$ is the velocity vector, w_s is the sediment settling velocity, and ε_d is the sediment eddy diffusivity.

Bed load transport was calculated using an approximation technique developed by van Rijn (2001). The direction and magnitude of the bed load at the cell centers was computed, followed by transport rates at the cell interfaces. The calculations took account of the effects of bed-slope, sediment availability and upwind bed composition. The sediment transport equations were solved by finite-volume methods.

* http://oss.deltares.nl/web/xbeach/. A model developed by the US Army Corps of Engineers, UNESCO-IHE, Deltares, Delft University of Technology and the University of Miami. Last access: 02 Feb 2016.

Sediment transport formulation of Van Rijn (2011)

There may be significant differences if different sediment transport relations are chosen, but adding another parameter to the set of tests here would only increase the complexity of the case so we decided to go with default relation of Delft3D (Van Rijn equation: VR).

$$S_T = S_b + S_S, \tag{2}$$

$$S_b = 0.006\rho_s w_s D_{50} M^{0.5} M_e^{0.7}, \tag{3}$$

$$S_S = 0.007 f_{SUSW} \gamma U_A \rho_s D_{50} M_e, \tag{4}$$

where S_T, S_b, S_S are the total, bed load and suspended sediment transport flux, respectively, D is the sediment diameter, M is the sediment mobility number due to waves and currents, M_e is the excess sediment mobility number, f_{SUSW} is a user-defined tuning parameter, γ (= 0.2) is the phase lag coefficient, and U_A is the velocity asymmetry value.

Boundary conditions

At the water surface, zero vertical diffusive flux of sediment was applied. At the bottom boundary, the net flux of sediments from the bed was calculated. The net flux in each computational cell was introduced to the bottom computational layer by means of a sediment source/sink term. At the lateral boundaries, the local equilibrium sediment concentration profile was used.

2.2 Numerical model setup

The model simulates a region of 1.3 km × 2.5 km in the cross-shore and longshore directions with constant initial cross-shore slope equate to alongshore uniform bathymetry at a site near Egmond aan zee (central part of the Dutch North Sea coast). The maximum water depth was 13 m and the maximum wind speed was about 20 ms^{-1} (perpendicular to shore). Figure 1 displays plan views of study area, bathymetry and computational mesh used in in the model domain. The van Rijn sediment formula (van Rijn 1993) and Chezy roughness formula with a Chezy value of 65 $m^{1/2}s^{-1}$ were used. The horizontal diffusivity and eddy viscosity were 0.5 and 1 m^2s^{-1}, correspondingly. The sediment density was 2.65 × 10^3 kg m^{-3} and the density of seawater was 1.025 × 10^3 kg m^{-3}. The size of grid was not constant (i.e., larger in the offshore area than near the beach). In the longshore direction, a smaller grid was selected in the central of the model domain, leaving a coarser grid in the outer areas on both sides. Based upon the rate of convergence, the grid cell size was selected to guarantee that the dependency of the numerical results on grid size is insignificant. The grid size selected changed between 10 m and 75 m per grid cell that allowed taking of alongshore currents. The initial time step was 3 s and it was decreased throughout the simulations based upon stability and convergence limitations.

Simulations were conducted using three initial bed slopes, four various turbulence models, and three oceanic forcing conditions. The median sediment diameters were 200, 500, 800, 1000 μm. In all cases, the model was run to simulate a one-month period. The figures display the final

bathymetry afterward the one month numerical simulations. A summary of the parameters for the scenarios simulated in the numerical experiments is reproduced in Table 1, where H is the wave height, A is the tidal amplitude, T is the wave period, D is the grain size, β is the bed slope, and α is the direction of wave propagation.

Table 1 Characteristics of the oceanic forcing and beach conditions in the numerical experiments (from Part I). Bold face indicates the base case and the parameter that is varied in each given subset of cases. The Van Rijn sediment transport formula was used in all cases

Case	H_s (m)	Tidal range (m)	D (μm)	T (s)	Oceanic condition	β	Turbulence closure model	α
1 (base case)	**2**	**2**	**200**	**7**	**wave + tide**	**1:100**	***k*-ε**	**260**
2	2	2	200	7	wave + tide	1:100	**H-LES**	260
3	2	2	200	7	wave + tide	1:100	***k*-*L***	260
4	2	2	200	7	wave + tide	1:100	**ATM**	260
5	2	-	200	7	**wave**	1:100	*k*-ε	260
6	-	2	200	-	**tide**	1:100	*k*-ε	-
7	**0.5**	2	200	7	wave + tide	1:100	*k*-ε	260
8	**1**	2	200	7	wave + tide	1:100	*k*-ε	260
9	**1.5**	2	200	7	wave + tide	1:100	*k*-ε	260
10	2	2	200	7	wave + tide	1:100	*k*-ε	**240**
11	2	2	200	7	wave + tide	1:100	*k*-ε	**280**
12	2	2	200	7	wave + tide	1:100	*k*-ε	**300**
13	2	**0.5**	200	7	wave + tide	1:100	*k*-ε	260
14	2	**1**	200	7	wave + tide	1:100	*k*-ε	260
15	2	**3**	200	7	wave + tide	1:100	*k*-ε	260
16	2	2	200	7	wave + tide	**1:50**	*k*-ε	260
17	2	2	200	7	wave + tide	**1:75**	*k*-ε	260
18	2	2	**500**	7	wave + tide	1:100	*k*-ε	260
19	2	2	**800**	7	wave + tide	1:100	*k*-ε	260
20	2	2	**1000**	7	wave + tide	1:100	*k*-ε	260

3. Results

We examined sediment transport processes and beach evolution by applying the 3D numerical model to various ocean and beach conditions. In §3.1, the simulated nearshore morphodynamics for the reference case are presented (Case 1), with nearshore morphologies predicted using different turbulence closure models given in §3.2 (Cases 1-4). The simulated morphodynamics for different oceanic forcing (Cases 1, 5, 6), various wave and tide characteristics (Cases 1, 7-15), and different beach characteristics (Cases 1, 16-20) are discussed in §3.3 to 3.5, respectively. The total sediment transport fluxes and volume changes in beach sediment for all the simulated cases are summarized in Table 2.

3.1 Predictions of nearshore morphodynamics: reference case

Fig. 2 shows a plan view of (a) cumulative erosion/sedimentation, (b) total sediment transport, (c) suspended sediment transport, and (d) vertical profile of sediment elevation for case 1. The primary morphodynamic response of the beach system consists of erosion in the wave-breaking zone and the deposition of sediment transported offshore to form a bar near the depth of closure (Fig. 2(a)). Sediment transport is mainly confined to the surf zone (Fig. 2(b)), with the breaking zone located at a cross-shore position of about 102.2 km [*Part I*]. High sediment concentrations in the water column occur in the inner surf zone where the entire water column is sediment-laden (Fig. 2(d)). Sediment concentrations reach maximal values near the bottom in the region, due to strong undertow [*Part I*]. The net change in sediment level over the offshore bar is comparable to level changes other sections of the foreshore (Fig. 2(a)), and sediment transport is less intense in the shoaling zone than in the surf zone (Figs. 2(b) and 2(d)).

Longshore variability is observed with the occurrence of a region of enhanced erosion at the breaking zone, just to the south of the seaward intrusion of the coastline at about 512.8 km north (Fig. 2(a)). A marked increase in significant wave heights and in current velocities was also observed at this location [*Part I*]. The occurrence of enhanced erosion in the breaking zone is accompanied by a reduction in the size of the offshore bar and the development of an intertidal bar at the same cross-shore location. The intertidal bar is discontinuous in the longshore direction. At the cross-shore position where the erosion zone extends furthest onshore, a low-relief area is observed between two sections of higher elevation. The formation of the intertidal bar is associated with erosion further up the beach face. The onshore extension of the beach is only apparent because the intertidal bar acts as a berm. The trough onshore of the intertidal bar is isolated from the rest of the nearshore zone and is characterized by quiescent hydrodynamics [*Part I*] and low sediment concentrations (Fig. 2(d)). Other intertidal bar and trough structures of smaller size are observed further north along the upper beach (Fig. 2(a)).

The cross-shore width of the zone of most intense sediment transport varies in the longshore direction (Fig. 2(b)) in a similar fashion to the current velocities (Figs. 6(a) and 6(b) of *Part I*) and surf zone width. The location of the maximum sediment transport rate along a cross-shore profile fluctuates with the longshore position. The cross-shore maximum is displaced onshore at the longshore position where the intertidal bar is formed (Fig. 2(b)). The intertidal bar also corresponds to the sediment transport maximum over the simulated domain. Bed load transport constitutes the main contribution to the total sediment transport over the intertidal bar (Figs. 2(b) and 2(c)), while suspended load constitutes most of the total load in the rest of the nearshore region.

Table 2 Sediment transport and beach evolution for all cases

Case	Cross-shore transport flux (m^2s^{-1})		Longshore transport flux (m^2s^{-1})		Cross-shore sediment volume (m^3)					
	Bed load	Suspended load	Bed load	Suspended load	Erosion (offshore: below the SWL)	Erosion (% of overall profile volume)	Deposition (onshore: above the SWL)	Deposition (% of overall profile volume)	Net	Net (% of overall profile volume)
1	2.96	37.77	0.016	-1.12	-8798	0.01872	3915	0.00833	-4883	0.01039
2	2.69	34.97	0.017	0.09	-10366	0.02206	3789	0.00806	-6578	0.01399
3	2.81	12.60	0.002	-1.08	-2891	0.00615	70310	0.14959	67418	0.14344
4	2.97	14.03	0.014	0.13	-5762	0.01226	78533	0.16709	72771	0.15483
5	3.30	35.48	0.018	0.97	-19587	0.04167	1273.1	0.00271	-18314	0.03897
6	0	0	0	0	-12	2.5×10^{-5}	0.4	8.5×10^{-7}	-11	2.3×10^{-5}
7	0.79	1.11	0.002	0.06	-2072.2	0.00441	1871.4	0.00398	-200.8	0.00043
8	1.95	7.20	0.007	0.36	-4584.8	0.00976	3790.3	0.00806	-794.5	0.00169
9	2.62	17.86	0.011	0.76	-6844.1	0.01456	5019	0.01068	-1825.1	0.00388
10	3.81	57.18	0.05	6.71	-29731	0.06326	1711	0.00364	-28020	0.05962
11	2.49	17.23	0.002	-2.10	-9652	0.02054	8870	0.01887	-782.2	0.00166
12	3.26	5.98	-0.006	1.24	-16193	0.03445	22726	0.04835	6532.5	0.01389
13	2.70	35.53	0.01	-2.69	2726	0.00580	6095	0.01297	3369	0.00717
14	2.88	36.74	0.016	0.33	-6270	0.01334	4645.1	0.00988	-1624.4	0.00346
15	3.57	33.42	0.019	1.92	-13361	0.02843	5136.4	0.01093	-8224.6	0.01749
16	3.89	42.72	0.017	-0.46	-7466	0.01589	27861	0.05928	20395	0.04339
17	3.51	41.35	0.02	1.09	-10616	0.02259	4163	0.00886	-6452	0.01373
18	3.72	2.46	0.017	0.06	-5611.9	0.01194	7416.2	0.01578	1804.3	0.00384
19	3.48	0.70	0.018	-0.001	-5228.5	0.01112	4829.3	0.01027	-399.2	0.00085
20	4.28	0.26	0.026	0.03	-2238	0.00476	1202.9	0.00256	-1035.1	0.00220

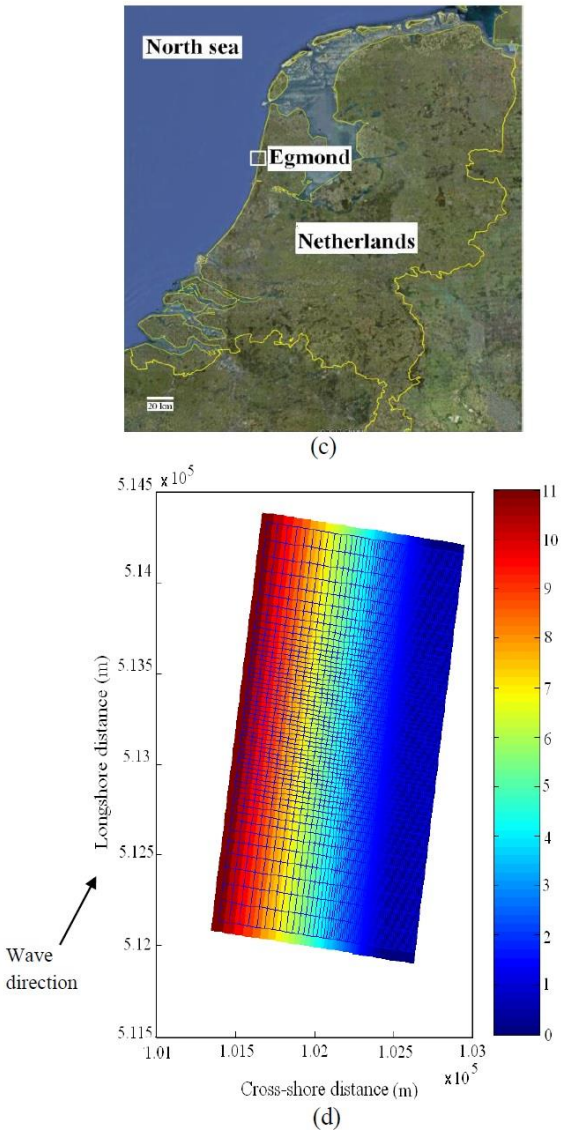

Fig. 1 (a) Plan view of study area (Egmond aan Zee, © Google 2015), and (b) bathymetry and computational mesh used in the case study at Egmond beach with the constant bed slope alongshore (after Part I)

The cross-shore distribution of bed load and suspended load in cross-shore and longshore directions is given in Fig. 3. Transport mainly occurs in the surf zone, with maxima on the upper beach and smaller fluxes in the shoaling zone. Cross-shore transport is almost exclusively offshore, with a maximum near the intertidal bar (Figs. 3(a) and 3(b)). The contribution of the suspended load to the total sediment flux is one to two orders of magnitude greater than the contribution of the bed load for both cross-shore (Figs. 3(a) and 3(b)) and longshore (Figs. 3(c) and 3(d)) fluxes.

Bed load transport is mostly cross-shore (Figs. 3(a) and 3(c)). The magnitude of the localized peak in longshore bed load transport at the intertidal bar is still only a small proportion of the average cross-shore bed load transport. The longshore suspended load flux in the upper beach region, near the intertidal bar, is more intense than and in the opposite direction to the longshore suspended flux in the outer surf zone, near the breaking zone (Fig. 3(d)). The reversal in the direction of suspended load longshore transport is likely related to the effect of nearshore recirculation cells on the distribution of horizontal velocity near the bottom.

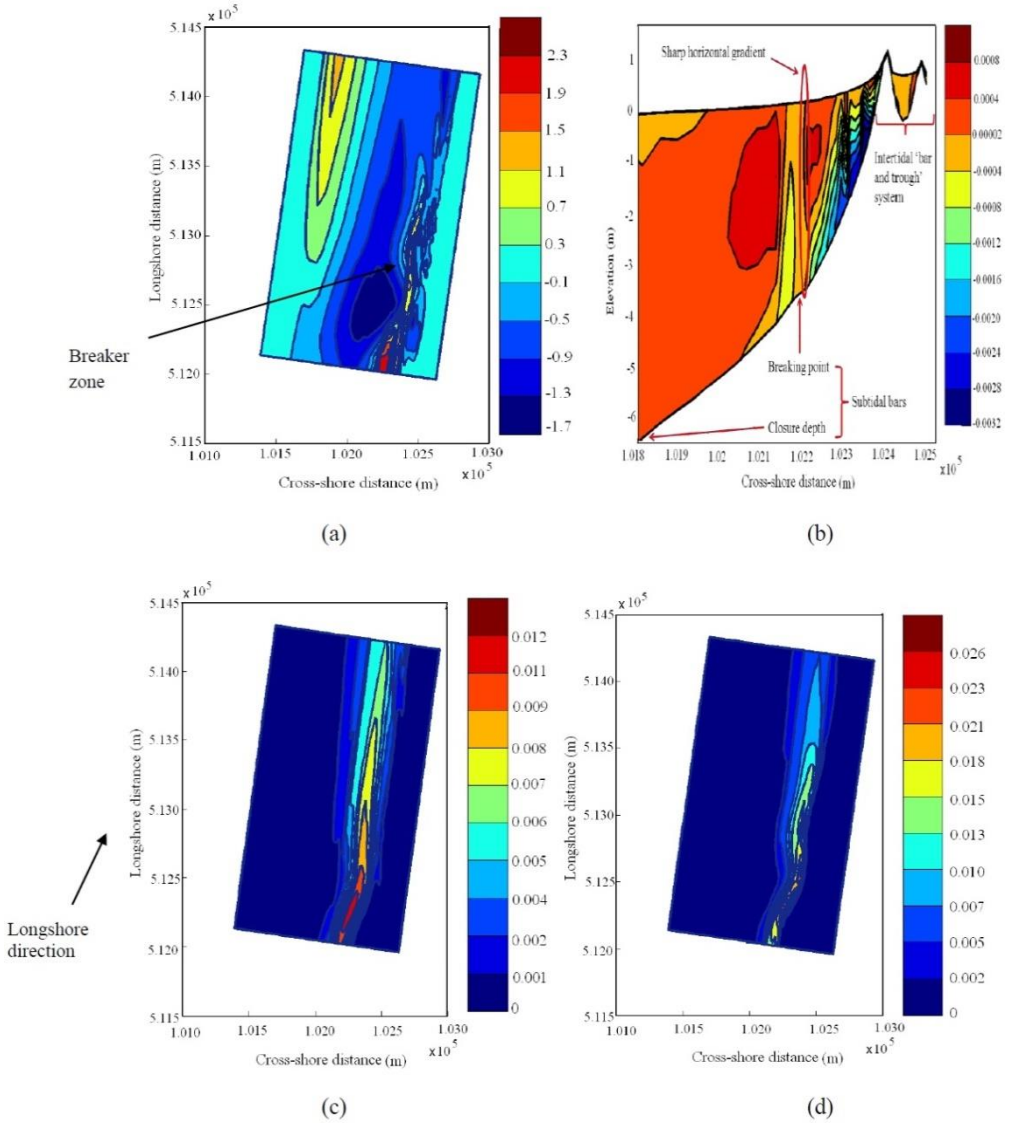

Continued-

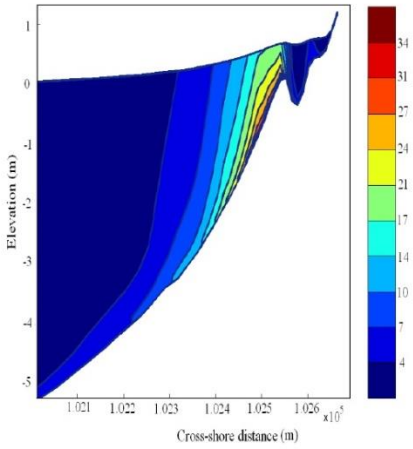

(e)

Fig. 2 Plan view of (a) cumulative erosion/sedimentation (m^3), (b) cross-shore distribution of vertical velocities (m/s, after Part I), (c) total sediment transport (m^2s^{-1}), (d) suspended sediment transport (m^2s^{-1}). (e) Vertical profile of sediment (m^3) for case 1 (β = 1:100, A = 2 m, α = 260 °, H = 2 m, combined wave and tide, k-ε turbulence model, D = 200 μm)

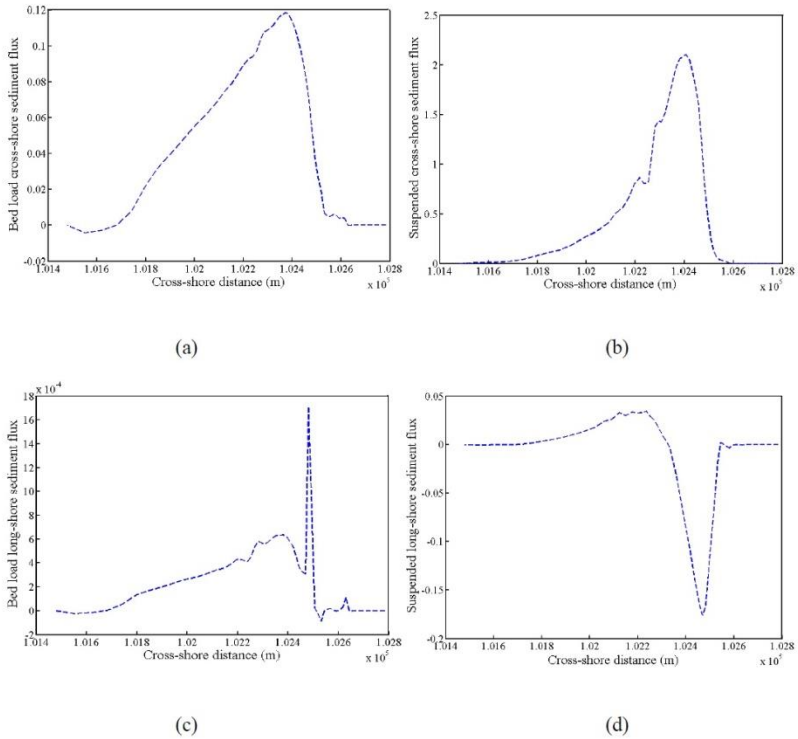

(a) (b)

(c) (d)

Fig. 3 Spatial distribution of (a) bed load in cross-shore, (b) suspended load in cross-shore and (c) bed load in longshore and (d) suspended load in longshore directions for case 1. Flux units are $m^3s^{-1}m^{-1}$

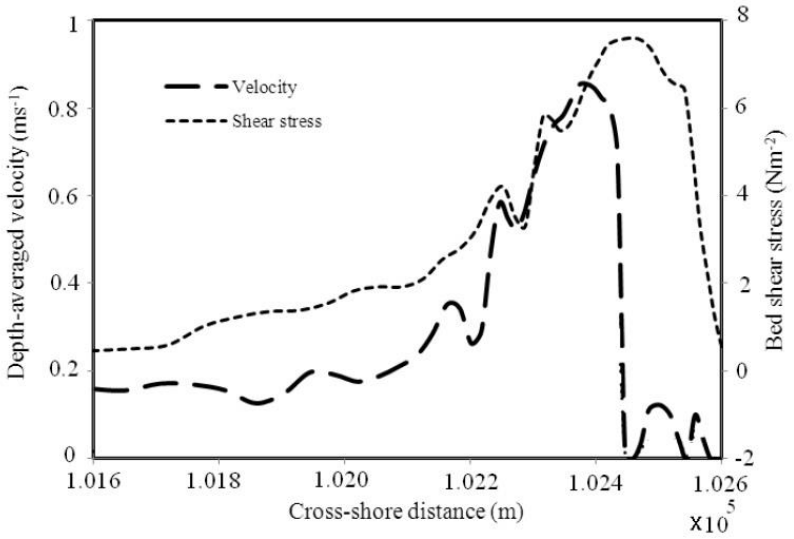

Fig. 4 Cross-shore variations of depth-averaged velocity and bed shear stress for case 1

The cross-shore variations of depth-averaged velocity and bed shear stress for case 1 are shown in Fig. 4. The velocity increases shoreward, incrementally in the shoaling zone and at a faster rate in the surf zone until it drops sharply at the base of the intertidal bar. The bed shear stress follows the same trend up to the intertidal bar, consistent with the observed return flow [*Part I*], but remains high shoreward of the intertidal bar and velocity peak. While the hydrodynamics in the trough onshore of the intertidal bar are, as expected, rather quiescent compared to the surf zone, the near-bottom velocity is still sufficiently large to generate a high bed shear stress. This is consistent with the large contribution of bed load transport to the overall sediment transport at that location (Figs. 3(b) and 3(c)). The entrainment threshold is exceeded by near-bottom flow but low velocities in the rest of the water column limit the suspended load.

3.2 Modeling of foreshore changes using different turbulence closure models

In this section, the numerical model was run with the four aforementioned turbulence closure models (cases 1-4). Nearshore morphodynamics predictions change with the turbulence model used (Elfrink and Baldock 2002, Bakhtyar *et al*. 2009d, 2010a, b). Turbulence is generated as waves reach shallow water and break, during which most of their energy is dissipated. Turbulence can stir up large quantities of sand, which remain in suspension for a number of seconds (van Rijn 2001). This sediment is carried along by the alongshore current. Littoral drift is particularly significant in the swash zone where re-suspended sediment tend to follow a zig-zag transport pattern (Masseling and Puleo 2009), resulting in beach drifting.

Changes in beach profile and cross-shore profile of sediment concentration are shown in Fig. 5. Sediment transport fluxes are displayed in Fig. 6 (Fig. 3 is for the reference case). Cross-shore and longshore fluxes are shown in the top and bottom panels, respectively. Bed load is on the left-hand panels and suspended load on the right. Where appropriate, the same two-figure presentation will

be used subsequently.

The beach profile evolution predicted with the H-LES model exhibits the same features as observed with the *k*-ε model: erosion in the breaking zone, deposition to form the offshore bar and formation of intertidal bar and trough structures (Fig. 5(a)). The intertidal bar for the H-LES model is not as developed as for the *k*-ε model, and the beach elevation is slightly higher in the rest of the foreshore profile. In fact, the upper beach profile after 500 h simulation with the *k*-ε model (Fig. 2) is closest to the profile predicted at the end of the simulation (720 h) with the H-LES model. Sediment concentration profiles (Fig. 5(b)) and sediment fluxes (Fig. 6) are similar between the two closure models. The only differences are the absence of a sharp peak in sediment concentration just over the intertidal bar in the H-LES case (Fig. 5(b)), a much lower longshore suspended load flux over the intertidal bar for H-LES compared to *k*-ε (Fig. 6(d)) and a minor offshore displacement of the maximum in concentration and peak fluxes. Such differences are consistent with the difference in size of the intertidal bar between the two cases.

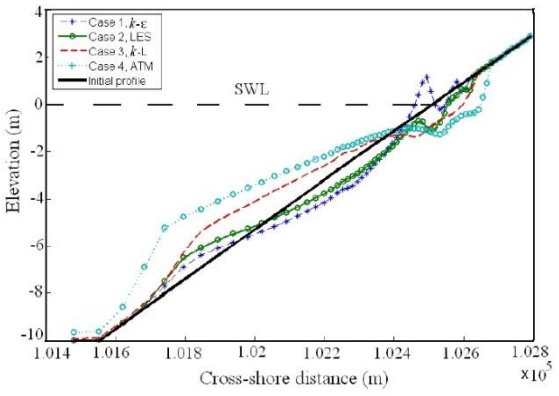

(a)

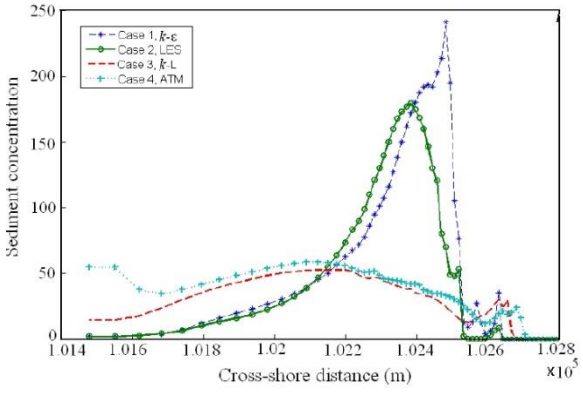

(b)

Fig. 5 Simulated (a) foreshore profile changes and (b) sediment concentration in the cross-shore direction for cases 1-4 (different turbulence models: listed in figures). The sediment concentration unit is mgl^{-1}

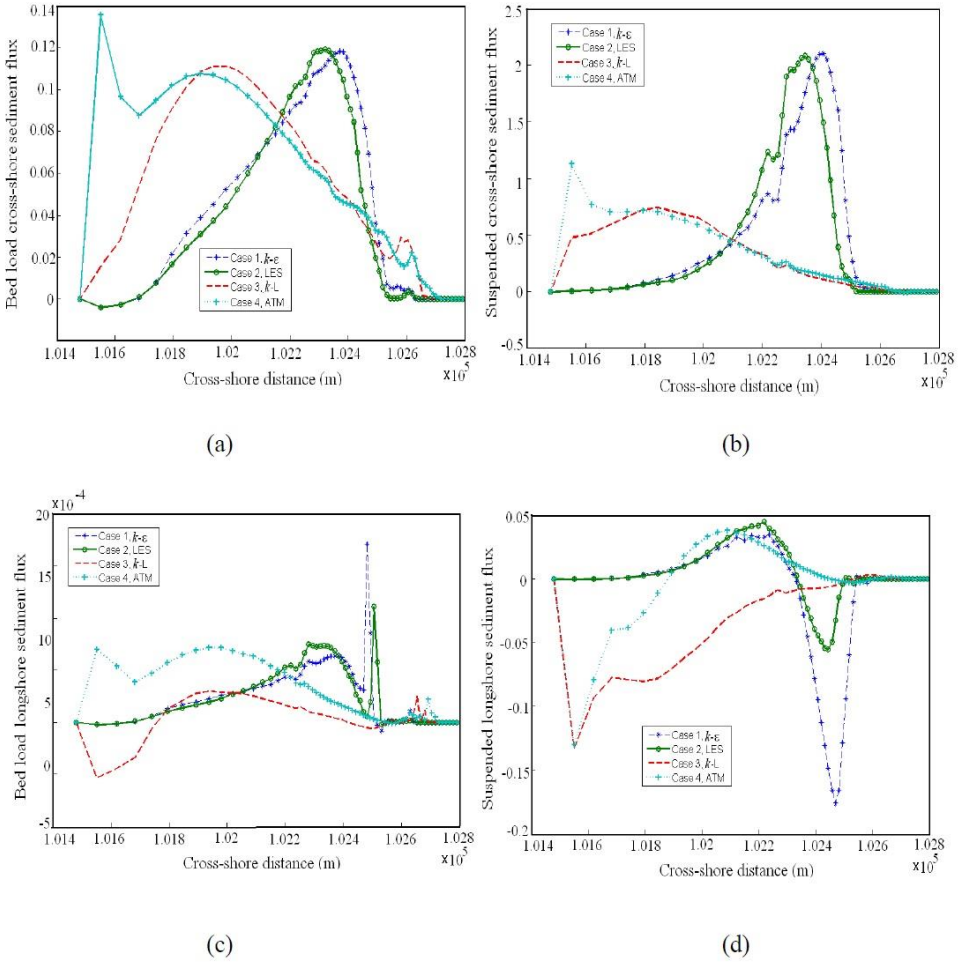

Fig. 6 Spatial distribution of (a) bed load and (b) suspended cross-shore sediment transport for cases 1-4 (different turbulence models: listed in figures). Cross-shore distribution of (c) bed load and (d) suspended LST for cases 1-4. Flux units are $m^3s^{-1}m^{-1}$

The morphodynamics predicted by the *k-L* and ATM turbulence closure models are very different from the results with *k*-ε and H-LES. Both *k-L* and ATM predict extensive accretion along most of the beach profile, with the exception of a narrow erosion zone in the upper beach (Fig. 5(a)). The accretion zone covers the equivalent of the entire beach profile from the wave-base up to the location of the intertidal bar that was obtained with the *k*-ε model. The erosion zone extends the immersed beach shoreward. Beach profile changes are more significant for ATM than for the *k-L* closure. The resulting profile is not concave upwards, but flat or slightly concave downwards, with a notch at the upper beach and a slope break offshore. Transport dynamics are dominated by the processes occurring over the accretion zone. The maximum sediment concentration is not a well-marked peak but rather a broad plateau spanning most of the beach (Fig. 5(b)). The cross-shore fluxes reach a maximum over the beach slope break (Figs. 6(a) and 6(b)). There is no

maximum in suspended longshore flux in the upper beach as with *k*-ε and H-LES (Fig. 6(d)). Longshore fluxes are different between ATM and *k*-*L*, which otherwise yield similar predictions. Bed load longshore fluxes are smaller in the *k*-*L* case compared to ATM, and they are in opposite directions offshore of the beach break (Fig. 6(c)). Suspended longshore fluxes are either in opposite directions or smaller in the ATM case compared with *k*-*L*, except offshore of the beach break (Fig. 6(d)). The fluxes predicted at the offshore boundary of the simulated domain tend toward non-zero values, sometimes even increasing. On the contrary, in the *k*-ε and H-LES cases, fluxes gently decay to zero and do not require being forced to zero at the boundary.

In applying the numerical models to real cases, there are a number of uncertainties, one of them is indeed the sedimentology of the study area and how it is represented in the model. Some research has been done on the effect of sediment mixtures on the (long term) morphological simulations and has provided suggestions and methods how to deal with these effect (Dastgheib *et al*. 2009, Van der Wegen *et al*. 2011). But including this effect in the paper will increase the complexity of the case to the extent that no knowledge can be gained for comparing all cases. In this paper, we have tried to use an idealized case to isolate the effects as much as possible to make the comparisons more reliable.

The *k*-ε and H-LES closure models yield similar results that are in better agreement with existing morphodynamic observations than the results of the other turbulent models investigated. Consistent with Part I, the 3D model associated with the *k*-ε model is used in the rest of present paper, as it is the most widely used (Lemos 1992, Christensen *et al*. 2002).

3.3 Modeling of foreshore changes for different oceanic forcing

This section examines the individual (cases 5 and 6) and combined (case 1) effects of tides and waves on nearshore morphodynamics. In the absence of waves, the numerical model predicts that the beach profile is unchanged (Fig. 7(a)) as there is no sediment transport (Figs. 7(a) and 8). This result is consistent with the predicted hydrodynamics where negligible flow velocities were observed in the tide-only case [*Part I*]. The numerical implementation of tidal forcing as an oscillation in the water level at the offshore domain boundary explains that tide alone has no effect on nearshore morphodynamics. Tidal currents generated as the tide propagates in coastal waters are not taken into account here.

Under wave forcing, the tidal fluctuations modulate the predicted nearshore sediment dynamics. Without the tide, the beach elevation is higher than under combined tide and wave forcing along most of the beach profile except in the upper beach (Fig. 7(a)). There is more accretion at the offshore bar, which is displaced onshore, and the erosion is reduced in the breaking and surf zones. The intertidal bar is replaced by a trough, thus extending the immersed beach. The berm in the wave-only case is located further onshore than the intertidal bar in the combined wave and tide case. The beach profile under waves only is similar to the profile predicted at 500 h simulation time with combined wave and tide forcing and to the profile in the H-LES case. The cross-shore profiles of sediment concentration and cross-shore fluxes of sediment transport are displaced onshore (Figs. 7(b), 8(a) and 8(b)), consistent with the shoreward shift observed in the overall beach profile and in the associated hydrodynamic characteristics (flow velocities, eddy viscosity, TDR, TKE, and flow setup) [*Part I*]. The reduction in the sediment concentration maximum observed in the upper beach (Fig. 7(b)), in addition to the overall onshore shift, indicates that the intensity of the peak in the combined case can be attributed to the presence of the intertidal bar.

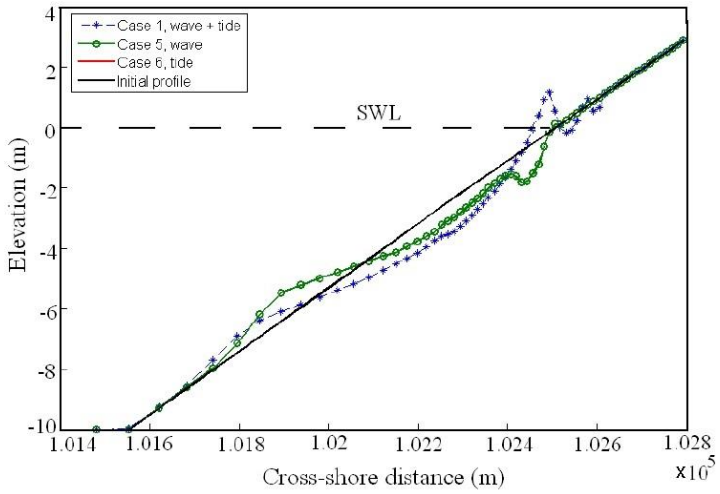

(a)

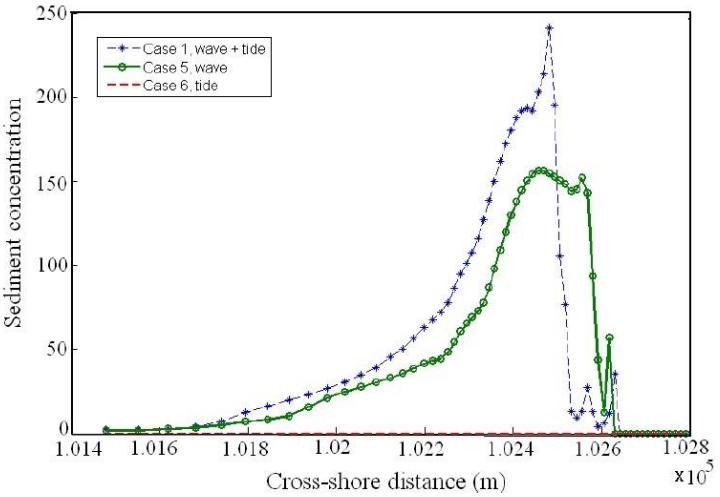

(b)

Fig. 7 Simulated (a) foreshore profile changes and (b) sediment concentration in the cross-shore direction for cases 1, 5 and 6 (different oceanic forcing: listed in figures). Sediment concentration units are mgl^{-1}

The addition of tidal forcing to wave action has a notable effect on longshore suspended sediment transport fluxes. The intense flux in the upper beach with a direction opposite to the flux around the breaking zone is no longer observed in the absence of the tide (Fig. 8(c)). This could be related to the asymmetry in the tidal signal that is noticeable in Figs. 3(a) and 4(a) of Part I. The difference in the intensity of the suspended longshore flux matches the reduction in sediment concentration noted on the upper beach. However, the reversal in longshore direction of the suspended load transport is not necessarily directly associated with the presence of the intertidal bar because the flux reversal in the upper beach is still observed in the H-LES case. With H-LES,

the intertidal bar is not developed and the sharp peak in sediment concentration is not observed, as in the wave-only case where there is no reversal.

These findings are consistent with existing understanding of the sediment transport processes in the nearshore zone (e.g., Cartier and Héquette 2011a): Laboratory observations showed that variation of LST is mainly controlled by obliquely wave breaking-induced currents (Komar and Inman 1970, Kamphuis 1991). However, in macrotidal areas (where the tidal range is 3 ~ 4 m), in addition to longshore currents generated by obliquely breaking waves, interactions of tidal currents with wave motions are important for sediment transport (Davidson *et al*. 1993, Cartier and Héquette 2011b).

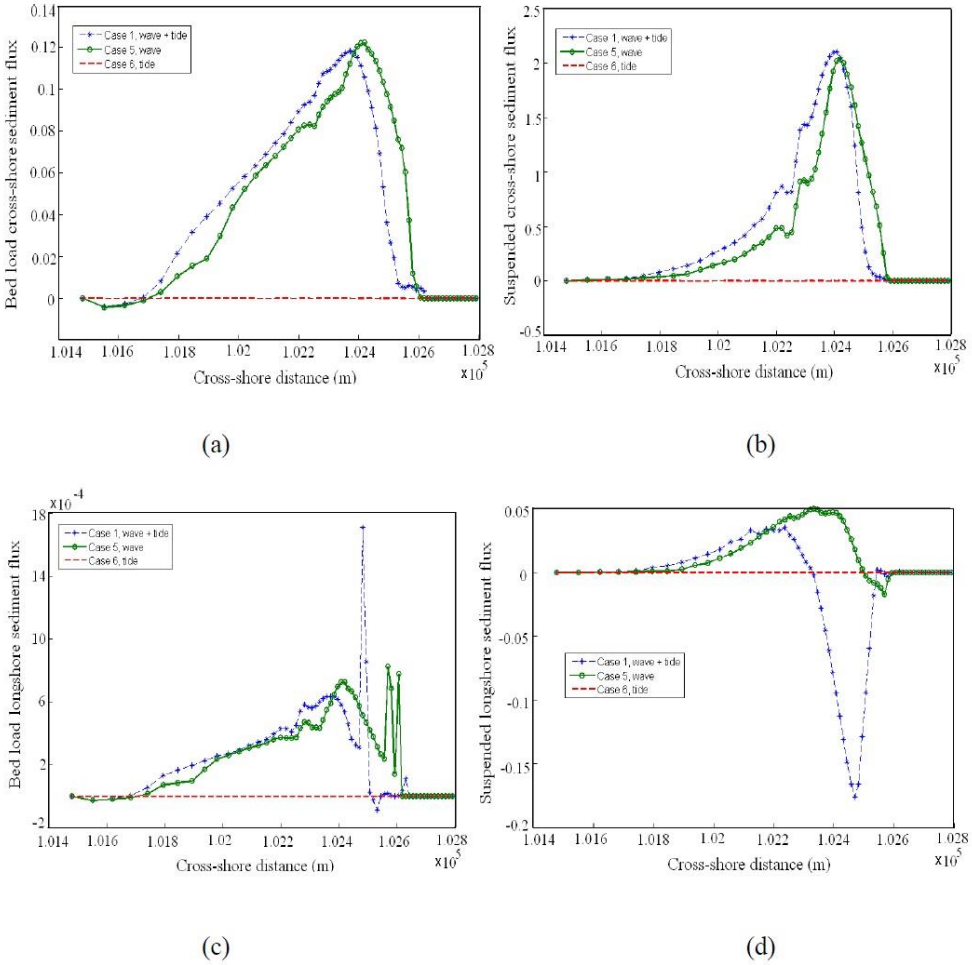

Fig. 8 Spatial distribution of (a) bed load and (b) suspended cross-shore sediment transport for cases 1, 5 and 6 (different oceanic forcing: listed in figures). Cross-shore distribution of (c) bed load and (d) suspended LST for cases 1, 5 and 6. Flux units are $m^3s^{-1}m^{-1}$

3.4 Effect of tide and wave characteristics on nearshore morphodynamics

One of the most important factors that govern the surf-swash motions and thus sediment transport is oceanic forcing energy (Karunarathna *et al*. 2005, Bakhtyar *et al*. 2012b). This energy is related to the wave and tide characteristics (viz., wave height, wave angle, and tidal range). In this section, nearshore morphodynamics are investigated numerically with different oceanic forcing characteristics (cases 1, 7-15).

Fig. 9(a) shows that, with increasing wave height, there is an increase in the change in foreshore profile, berm size and volume of transported sediments. Beach profile patterns for cases 7-9 are the same, with erosion above the SWL and generation of a bar below it, while the beach profile for case 1 (largest wave height) shows a different pattern (deposition above the SWL and large erosion area below). Fig. 9(b) reveals that maximum sediment transport and sediment concentration take place near the breaking area, and then decrease towards the shore (compare maximum sediment concentrations for various cases in panel b). Moreover, waves break sooner for larger wave heights.

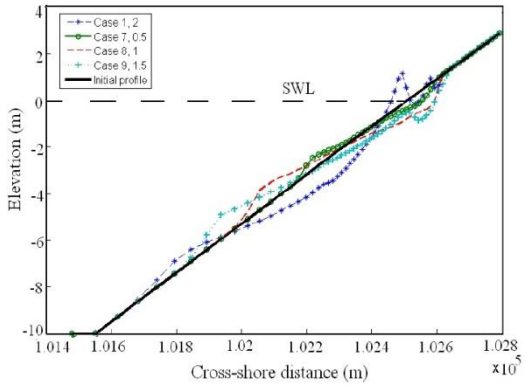

(a)

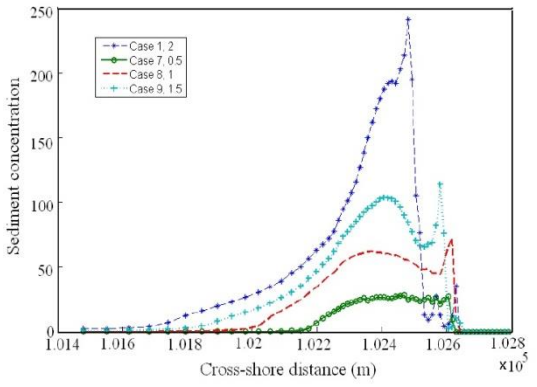

(b)

Fig. 9 Simulated (a) foreshore profile changes and (b) sediment concentration for cases 1 and 7-9 (different wave heights: listed in figures). Sediment concentration units are mgl^{-1}

Fig. 10 depicts the spatial distribution of bed load and suspended cross/longshore sediment transport for different wave heights. It can be observed from Fig. 10(b) that the maximum of the bed load cross/longshore sediment flux shifts upward and off-shoreward with increasing wave height (Fig. 10(a) and 10(c)). Fig. 10(b) and (d) show that the suspended cross/longshore sediment fluxes are noticeably greater for case 1 (largest wave height corresponded to higher wave energy). For the smaller wave height (low wave energy conditions), the surf zone width is decreased and, beyond the breaker zone, sediment fluxes generally consist of LST driven by tidal currents (Cartier and Héquette 2011a). Therefore, because of less tidal-induced sediment resuspension, low sediment transport occurs. These outcomes are consistent with prevailing understanding of the nearshore morphodynamics (USACE, 1984, Bayram *et al*. 2007). The highest sediment flux for case 1 is an order of magnitude greater than that for case 7, which displays the significance of wave height on the beach morphodynamics.

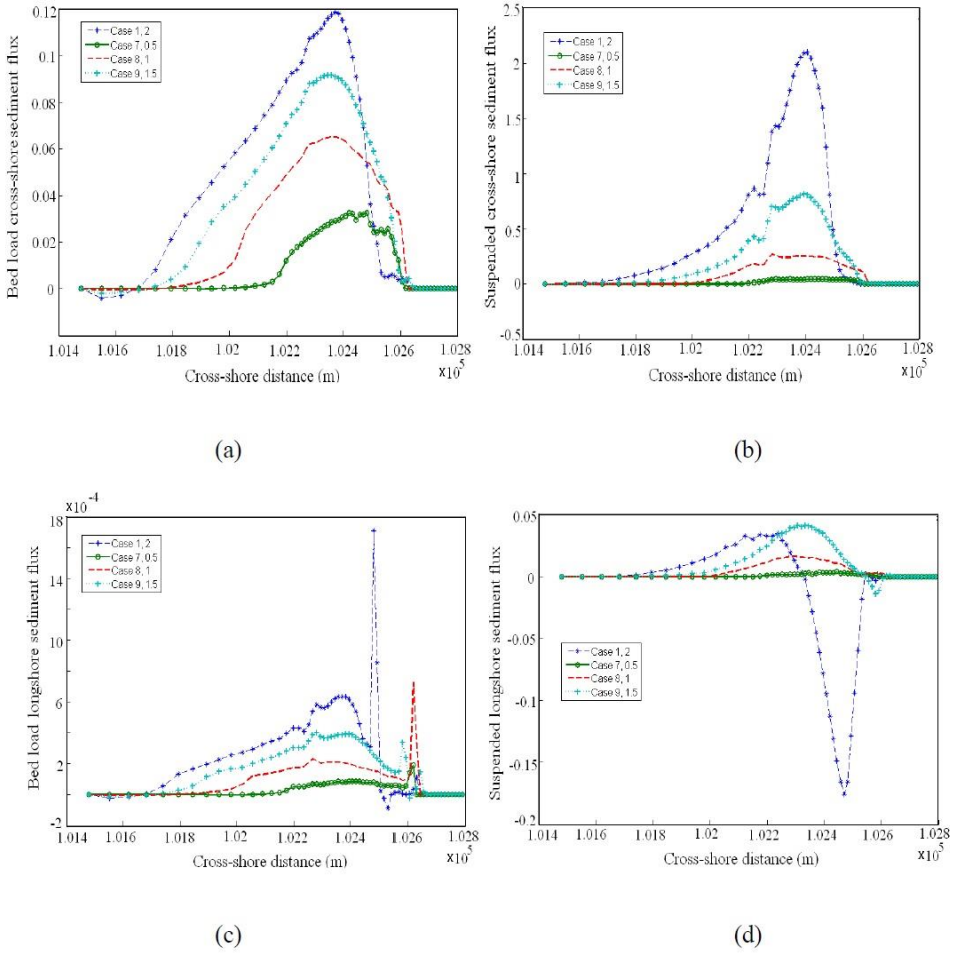

Fig. 10 Spatial distribution of (a) bed load and (b) suspended cross-shore sediment transport for cases 1 and 7-9. Cross-shore distribution of (c) bed load and (d) suspended LST for cases 1 and 7-9 (different wave heights: listed in figures). Flux units are $m^3s^{-1}m^{-1}$

Wave motions and breaking that propagate obliquely to the beach generate both cross/longshore currents and play a substantial role in sediment transport (Longuet-Higgins 1970). These processes are strongly dependent on wave angle. Fig. 11 displays that, with increasing wave angle, foreshore profile changes, berm size and volume of transported sediments decrease. Fig. 12 shows that both bed- and suspended sediment fluxes in both cross- and longshore directions decrease with increasing wave angle.

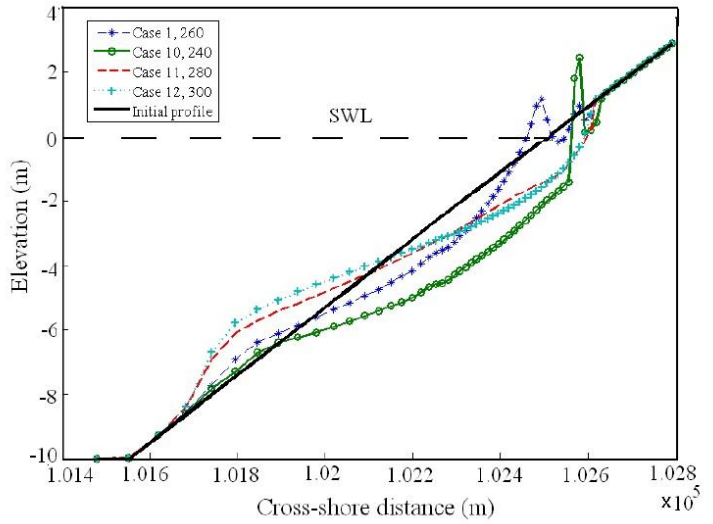

(a)

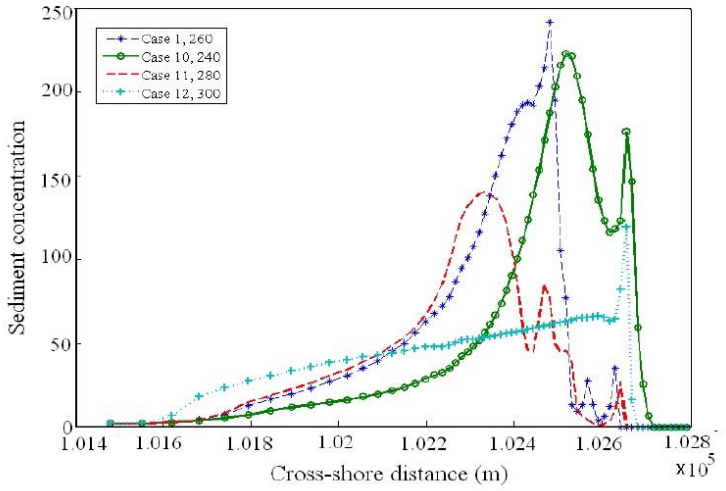

(b)

Fig. 11 Simulated (a) foreshore profile changes and (b) sediment concentration for cases 1 and 10-12 (different wave angles: listed in figures). Sediment concentration units are mgl^{-1}

Interactions between tide and wave can affect the nearshore hydrodynamics and morphodynamics (*Pattiaratchi and Collins*, 1984). The main effect of tide in the morphodynamics of this case is the changing location of the breaking wave during different phases of the tide; the wave imposed in the model breaks in different cross-shore locations, and affects the morphological evolution of the beach. As it is seen in Fig. 7(a), the tide with the low amplitude, similar to what is used in this simulation, do not have a lot of effect on the beach morphology; but when wave is added the tide shows its effect by moving the breaker zone onshore and offshore, resulting in a wider breaking zone, and higher nearshore bar. In spite of its significance, detailed simulation of combined waves and tides is not often conducted. This is because hydrodynamics of waves and tides are complex and act on different time scales (Xin *et al*. 2010, Bakhtyar *et al*. 2013a).

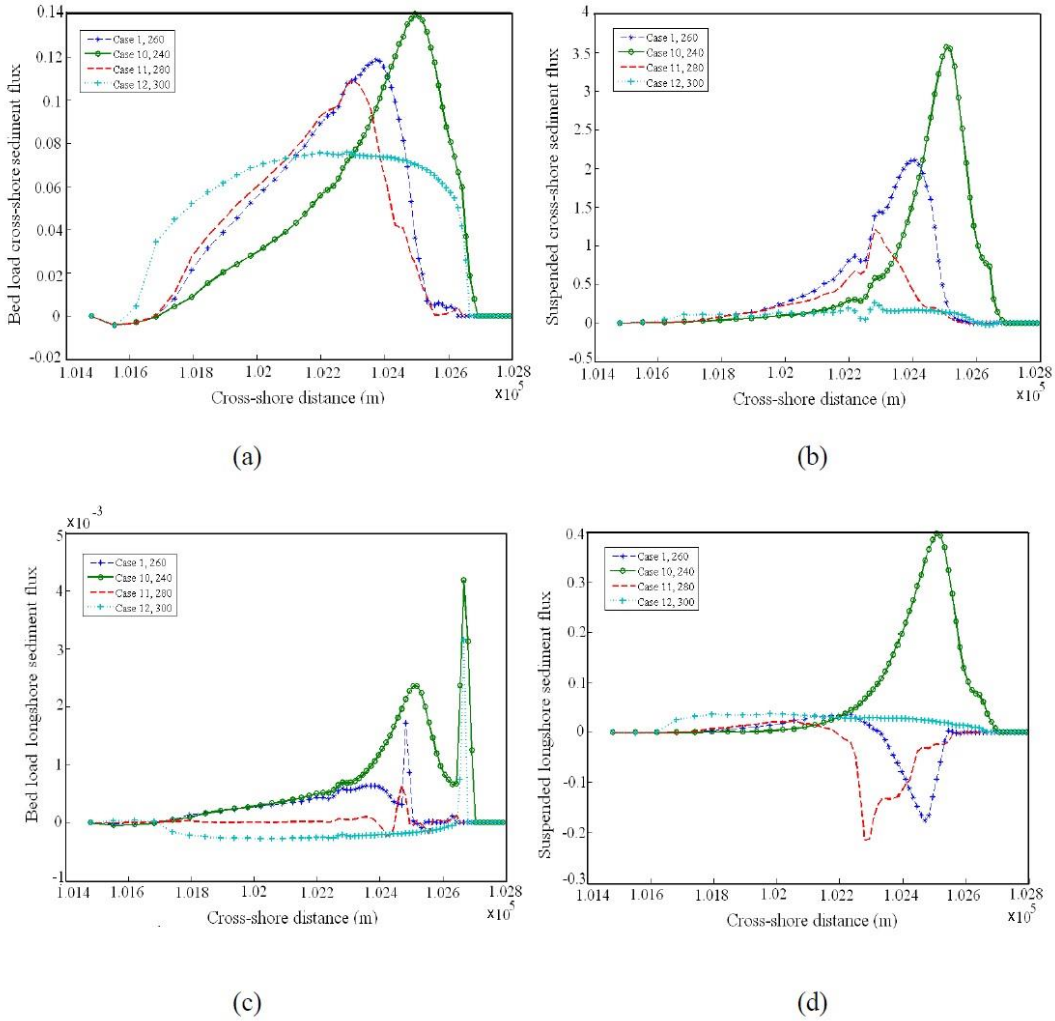

Fig. 12 Spatial distribution of (a) bed load and (b) suspended cross-shore sediment transport for cases 1 and 10-12 (different wave angles: listed in figures). Cross-shore distribution of (c) bed load and (d) suspended LST for cases 1 and 10-12. Flux units are $m^3s^{-1}m^{-1}$

Foreshore profile changes and sediment concentration for cases with different tidal ranges are given in Fig. 13. Fig. 7, in agreement (Trim *et al*. 2002), shows that tidal forcing alone is not sufficient to drive sediment circulation and formation of the bar and berm. However, Fig. 13 shows that tidal amplitude is important for the combined wave and tide cases. Fig. 14 shows that, with increasing the tidal amplitude, both bed load and suspended sediment flux decrease. A comparison of Figs. 11 and 13 shows that the wave height is a more important factor than tidal range to determine the beach profile changes. Sediment transport in the nearshore region is dependent on wave energy (Karunarathna *et al*. 2005, Bakhtyar *et al*. 2010, 2012b). Since wave energy is proportional to the square of wave height, higher waves induce a greater sediment flux. Furthermore, the surf zone width increases as the wave height and wave energy increase, and a larger bar is generated (Hughes and Chiu 1981). For the tidal case, a very small volume of material was transported and did not cause considerable changes in the beach profile. This is because, under tidal forcing, TKE, flow velocity, and energy are low during both flood- and ebb- tide, and sediment resuspension is less. However, simulations that neglect the effects of tides are unable to reproduce accurately beach evolution when waves are present.

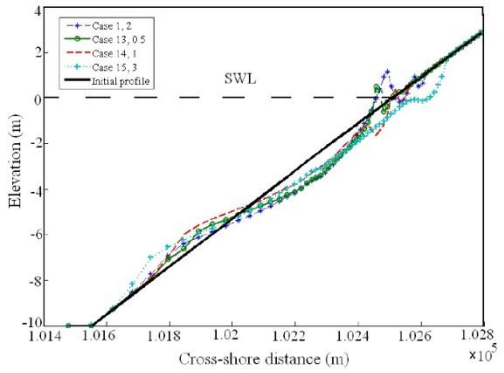

(a)

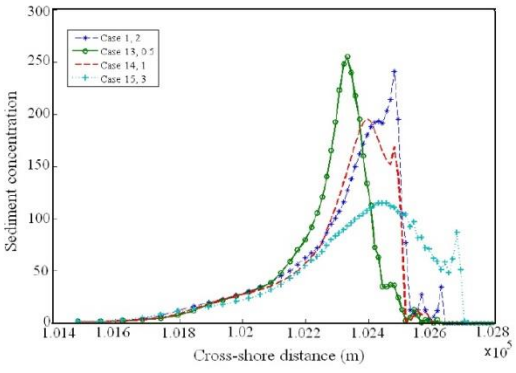

(b)

Fig. 13 Simulated (a) foreshore profile changes and (b) sediment concentration for cases 1 and 13-15 (different tidal ranges: listed in figures). Sediment concentration units are mgl^{-1}

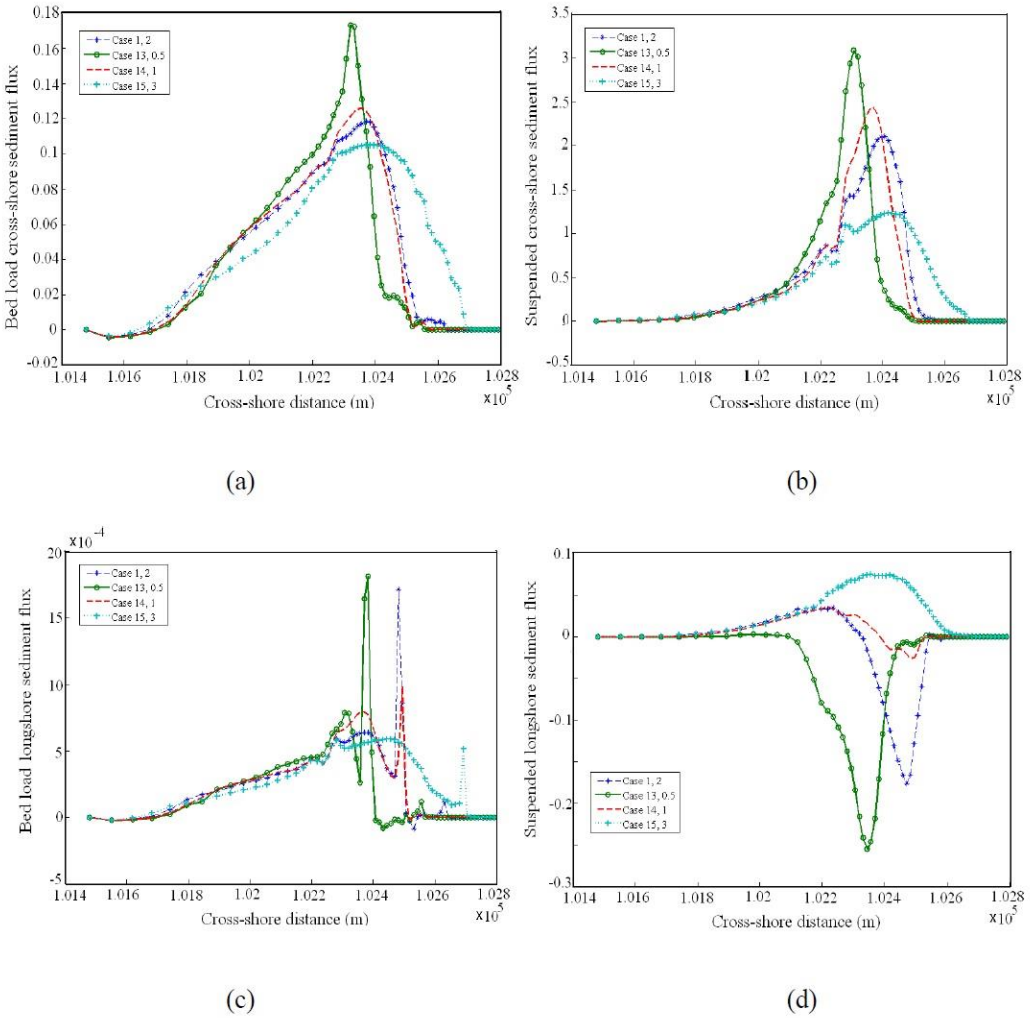

Fig. 14 Spatial distribution of (a) bed load and (b) suspended cross-shore sediment transport for cases 1 and 13-15. Cross-shore distribution of (c) bed load and (d) suspended LST for cases 1 and 13-15 (different tidal ranges: listed in figures). Flux units are $m^3s^{-1}m^{-1}$

3.5 Influence of beach characteristics on nearshore morphology

Beach type and corresponding wave breaking type can be classified into two categories (Aagaard and Hughes 2006): (i) intermediate beach and plunging breakers (steep beaches) and (ii) dissipative beach and spilling breakers (gentle beaches). Two major parameters that determine the beach type are sediment grain size and beach slope (Miles *et al*. 2006, Bakhtyar *et al*. 2012a, b). Numerical simulations were run for different beach slopes and for a range from coarse to fine sand beaches (cases 1, 16-20).

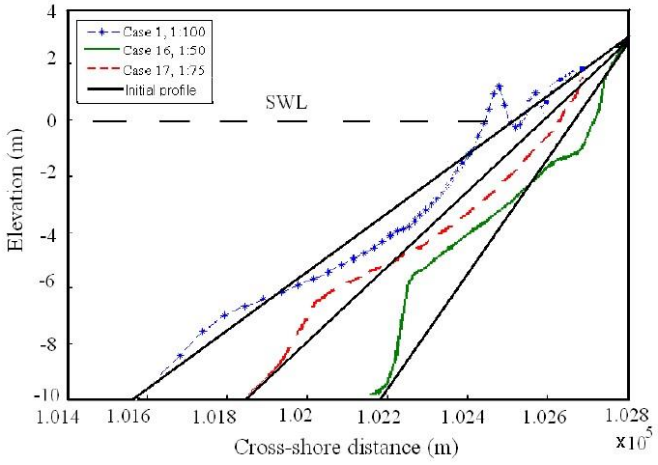

(a)

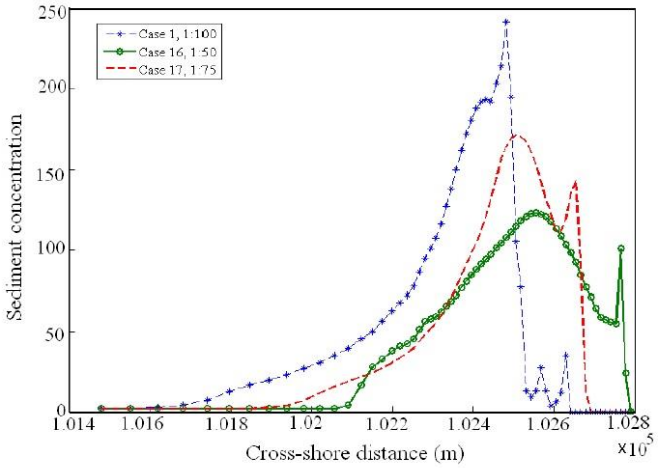

(b)

Fig. 15 Simulated (a) foreshore profile changes and (b) sediment concentration in the cross-shore direction for cases 1, 16 and 17 (different bed slopes: listed in figures). Sediment concentration units are mgl^{-1}

Predicted beach profiles for different bed slopes (cases 1, 16 and 17) in the cross-shore direction are shown in Fig. 15. The results show that, in the cross-shore direction and for steeper beaches relative to milder beaches, the berm and bar sizes and beach profile change and are greater, and sediment transport flux is larger. This is due to several factors such as (Trim *et al.* 2002): (i) on the steeper beach, wave breaking occurs further onshore, therefore the wave energy is increased in the nearshore zone, (ii) as beach slope increases, the return flow and undertow velocity increases, which is important for sediment transport in the surf zone (Masselink and Black 1995), (iii) on

steeper beaches, the required velocity magnitude for initiation of sediment motion decreases (because bed slope is close to sediment angle of repose), (iv) on steeper slopes, the swash depth is larger than that on milder slope; therefore the governing mode of sediment transport is in suspension, so that sediments remain in the water column and are transported offshore by the undertow (Horn and Mason 1994). In the longshore direction, the sediment transport flux is larger for more gentle beaches. The zig-zag pattern in the swash zone is most relevant under low-energy conditions, generally associated with a gentle beach profiles.

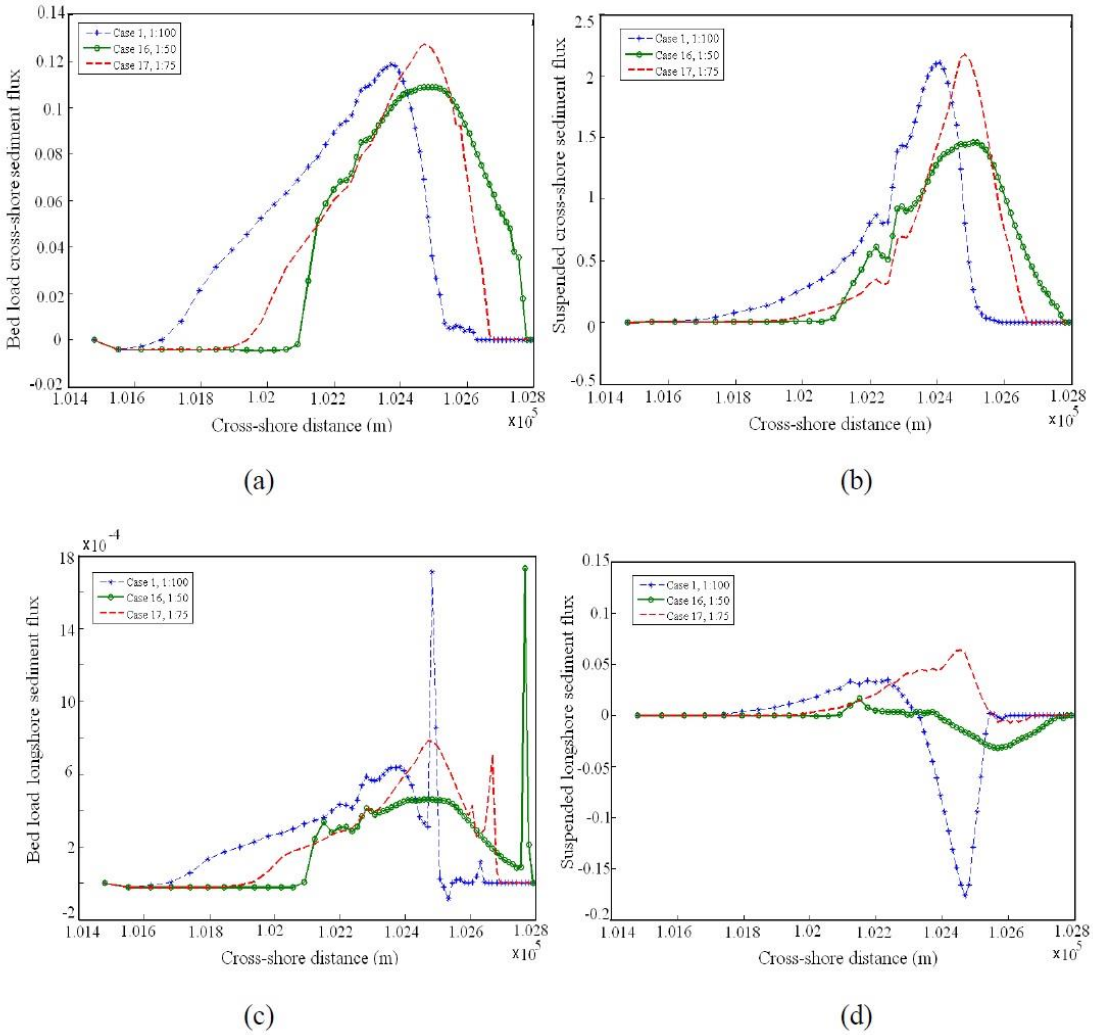

Fig. 16 Spatial distribution of (a) bed load and (b) suspended cross-shore sediment transport for cases 1 and 16-18. Cross-shore distribution of (c) bed load and (d) suspended LST for cases 1, 16 and 17 (different bed slopes: listed in figures). Flux units are $m^3s^{-1}m^{-1}$

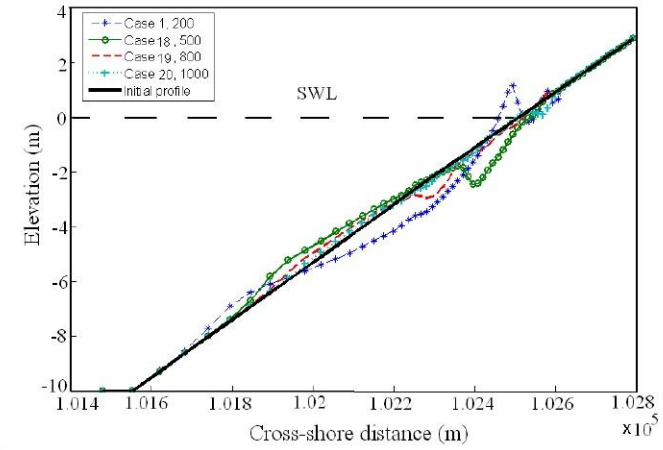

(a)

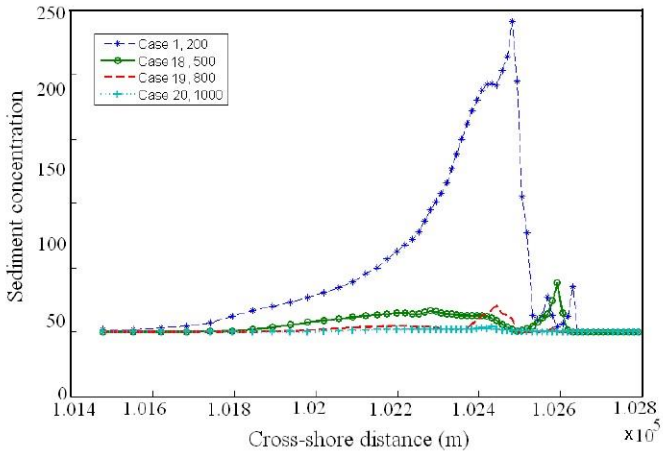

(b)

Fig. 17 Simulated (a) foreshore profile changes and (a) sediment concentration in the cross-shore direction for cases 1 and 18-20 (different grain sizes: listed in figures). Sediment concentration units are mgl^{-1}

Figs. 17(a) and 17(b) show foreshore profile changes and sediment concentration in the cross-shore direction for different grain sizes. Simulated beach profiles show different deposition and erosion shapes on the beach face. The predicted profile for the finest sand (case 1) reveals deposition and generation of a berm above the SWL and erosion and formation of bar beneath it. By increasing the sediment size, the volume of sediment transport and changes in beach profile

decrease. For coarser grain sizes, erosion occurs on the upper beach face and bars form on the lower part of beach face. Furthermore, a comparison between the four grain sizes shows that when the sediment diameter is small, the sediment transport rate is large (panel b). The maximum sediment transport is found near the breaking point and close to shoreline (cross-shore distance near 1.025×10^5 m, Fig. 17(b)).

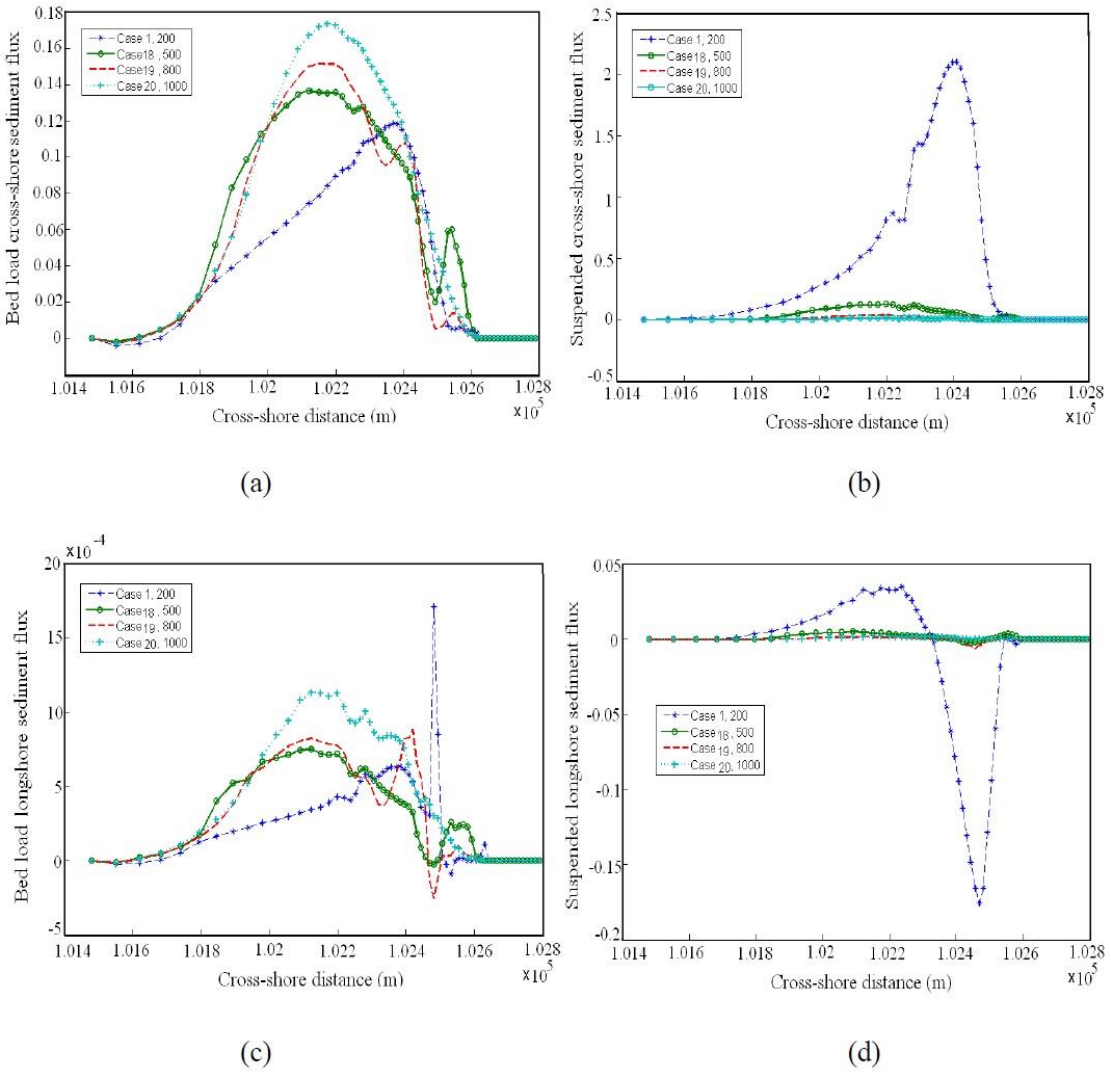

Fig. 18 Spatial distribution of (a) bed load and (b) suspended cross-shore sediment transport for cases 1 and 19-21. Cross-shore distribution of (c) bed load and (d) suspended LST for cases 1 and 18-20 (different grain sizes: listed in figures). Flux units are $m^3s^{-1}m^{-1}$

A comparison between the sediment transport flux in cross-shore and longshore directions shows that the sediment flux in the cross-shore direction is two orders of magnitude larger than that in the longshore direction (Fig. 18). In addition, in both directions, the suspended sediment flux is larger than the bed load flux. This may due to the different settling velocities: Small grains are entrained after wave breaking and swash motion, but they do not have enough time to return to the bed. Therefore, through the long/cross-shore currents, the grains in the water column are suspended and transported. While bed load and suspended sediment flux for the four grain size show a similar pattern, there are dissimilarities in the magnitude and position of maximum sediment flux. Sediment concentration and suspended sediment fluxes are significantly larger in the reference case than in the other three cases with larger grain sizes, for which concentration and fluxes are comparable (Figs. 17(b), 18(b) and 18(d)). Conversely, bed load transport occurs over a reduced section along the upper beach profile for the smaller grain size compared to the larger sizes where significant bed load fluxes are sustained over wider portion of the beach profile (Figs. 18(a) and 18(c)). Coarser grain sizes form a group that is distinct from the reference case with respect to sediment transport.

Sediment travel distance depends on sediment size. Coarser sediments move less and are more often transported as bed load than suspended load. An indication of the horizontal to vertical travel ratio, $\Delta x/\Delta y$, is given by (Le Méhauté, 1970) U_p/w_s, where U_p is the horizontal peak velocity and w_s is the terminal velocity. Stokes law is not valid to estimate the terminal (settling) velocity. Here, the expression of Ferguson and Church (2004) was used, which expresses settling velocity as a function of sediment size

$$w_s = \frac{RgD^2}{C_1 v + \left(0.75 C_2 RgD^3\right)^{1/2}}, \tag{5}$$

where R is the submerged specific gravity, g is the magnitude of gravitational acceleration and v is the kinematic viscosity of the fluid. For natural sand grains, Ferguson and Church (2004) recommend $C_1 = 20$ and $C_2 = 1.1$. For the different sediment sizes used in the present study (i.e., D = 0.2, 0.5, 0.8, 1 mm), $\Delta x/\Delta y$ = 32.25, 11.11, 7.52, 6.41, respectively. The ratio for the reference case is 3 to 4 times larger than for all the other simulated cases, which have similar ratios. This is consistent with model predictions. There seems to be a threshold value for the travel ratio (roughly between 10 and 30, and thus between 0.2 and 0.5 mm for grain sizes) separating two distinct types of sediment transport configurations. Finally, within the group of coarser grains, the travel ratio varies very little as the grain size increases. The results for suspended load fluxes show no discernible differences between the largest two sizes.

4. Discussion

Summary plots showing the effects of selected parameters on sediment transport fluxes and flux ratios are presented in Figs. 19 and 20. Flux predictions for all the numerical experiments of a given series are plotted against the varying parameter in the series. The best linear fit to each series is provided for physical variables. Sediment transport fluxes are mostly occurring in the cross-shore direction (Fig. 19(f)). Waves are the dominant forcing controlling sediment transport fluxes (Fig. 19(f)). Consistently, wave height yields the best fit of all parameters with both cross-shore and longshore sediment fluxes (Fig. 19(b)), as well as a good fit with onshore to

offshore and longshore to cross-shore flux ratios (Fig. 20(a)). Net fluxes increase with increasing wave height (Fig. 19(b)). Decreasing wave height increases the proportion of onshore to offshore fluxes, almost reaching a neutral net balance (Fig. 20(a)). Seasonal variability in wave climate is known to affect the equilibrium beach profile (Saravanan and Chandrasekar 2010, Ruggiero *et al*. 2010). Steep profiles are observed in winter under large waves with high erosive power while summer profiles are gentler as smaller waves induce onshore sediment transport (Dail *et al.* 2000, Yates *et al.* 2011).

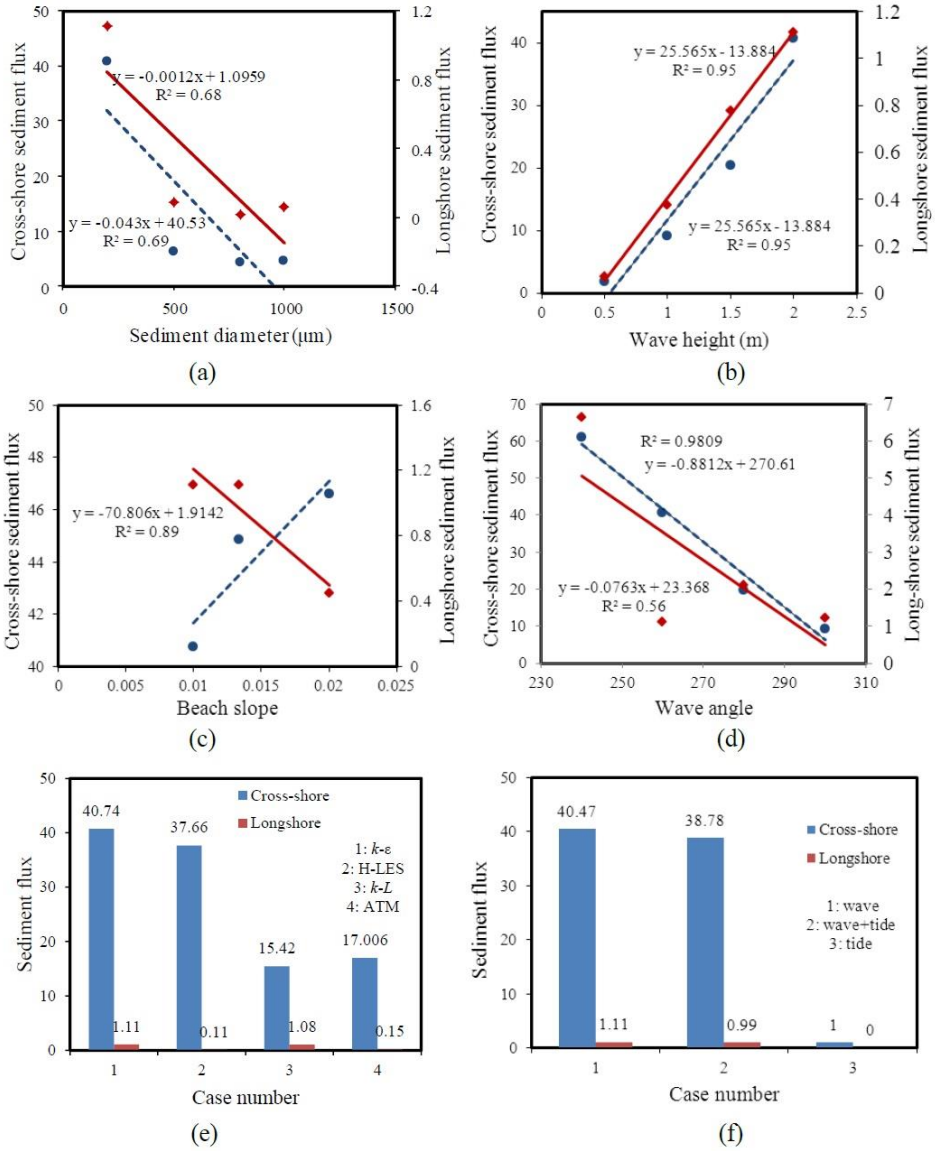

Fig. 19 Cross-shore and longshore sediment flux vs. (a) sediment diameter, (b) wave height, (c) beach slope, (d) wave angle. Cross and longshore sediment fluxes for (e) different turbulence closure models, and (f) different oceanic forcing. Blue circles are cross-shore sediment and red squares are longshore flux. Flux units are $m^3s^{-1}m^{-1}$

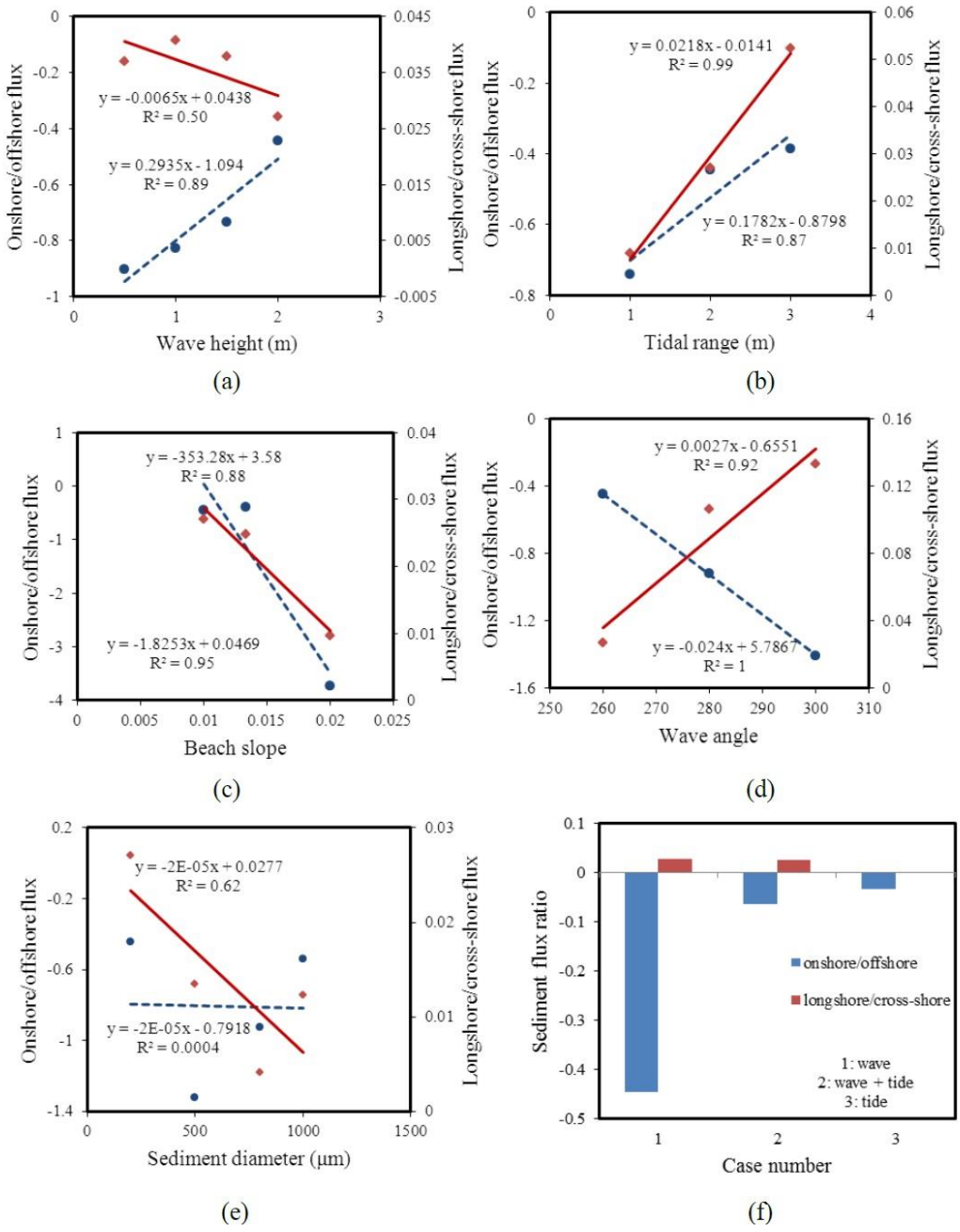

Fig. 20 Onshore/offshore and longshore/cross-shore sediment flux ratio vs. (a) wave height, (b) tidal amplitude, (c) beach slope, (d) wave angle, (e) sediment diameter. (f) Onshore/offshore and longshore/cross-shore sediment flux ratio for different oceanic forcing. Blue circles are cross-shore sediment and red square symbols are alongshore flux

Under wave action, tidal forcing affects the beach sediment budget by increasing the predominance of offshore over onshore transport (Fig. 20(f)) by a factor of 10. Accordingly, the increasing linear fit of the tidal range to the onshore-to-offshore flux ratio is convincing (Fig. 20(b)). Large tidal ranges enhance longshore with respect to cross-shore fluxes, although the latter remains predominant (Fig. 20(b)).

The dependence of cross-shore sediment fluxes on wave angle is well described by a decreasing linear fit (Fig. 19(d)). Net cross-shore fluxes revert from offshore to onshore with increasing wave angle. The relative contribution of longshore versus cross-shore fluxes increases (Fig. 20(d)). As the wave angle increases, the longshore flux varies non-monotonically, perhaps indicating some symmetry around a direction of maximum longshore flux near the normal incidence to the shoreline (Fig. 19(d)). Sediment fluxes have a non-linear dependence on grain size (Fig. 19(a)), with a threshold between 0.2 and 0.5 mm. Fluxes strongly increase below the threshold, as expected with sediment entrainment laws following Bagnold's energetics approach where transport is a high-order function of excess Shields number (ratio of shear stress to gravity effects, inversely proportional to grain size). Beach slope has a consistent effect – there is a well-defined increase in cross-shore sediment transport flux as the beach gets steeper.

5. Conclusions

Part I of this paper describes 3D hydrodynamic models under different beach types and oceanic forcing. Part II presents results of this model for sediment transport and beach morphology.

The simulations showed that wave forcing alone is sufficient to drive a sediment circulation pattern that results in bar and berm formation. The addition of tidal forcing to wave action has a notable effect on longshore suspended sediment transport fluxes. Numerical results showed that the k-ε and H-LES closure models give more reasonable results (consistent with existing morphodynamic understanding) than the results of the other turbulence models. The results of the 3D model confirmed that the wave energy, beach grain size and bed slope are main factors affecting erosion/deposition, bed load and suspended load, and cross-shore and LST in the nearshore zone. In addition, for the same type of oceanic forcing, the beach morphology exhibits different erosive characteristics depending on grain size. Coarse- and fine-sand beaches differ significantly in their erosive characteristics (e.g., foreshore profile evolution is erosive and accretionary on the fine and coarse sand beaches, respectively), while net cross-shore fluxes revert from offshore to onshore with increasing wave angle. Decreasing wave height increases the proportion of onshore to offshore fluxes, almost reaching a neutral net balance. After one month (simulation time), the bathymetry is strongly non-uniform. The non-uniform resulting bathymetry is due to generation of two bars, and as soon as the initial bars start to grow it affects the flow field which again feeds back to the morphological changes. Beach profile steepness modifies the nearshore circulation pattern, significantly enhancing the vertical component of the flow. As the steepness increases; TKE, sediment concentrations and transport increase and there are several occurrences of plunging flow in the upper half of the water column in the foreshore. The numerical model results show that present process-based model is capable of simulating the hydro- and morpho-dynamics in both cross- and along-shore directions, providing results in reasonably good agreement with current understanding of beach processes.

Acknowledgments

Support of the Swiss National Foundation (SNF 200021-135322) is acknowledged.

The authors would like to thank Dr. N. Le Dantec for his careful review of the manuscript and the suggestions he made.

References

Aagaard, T. and Hughes, M.G. (2006), "Sediment suspension and turbulence in the swash zone of dissipative beaches", *Mar. Geol*., **228**(1-4), 117-135.

Antuono, M., Brocchini, M. and Grosso, G. (2007), "Integral properties of the swash zone and averaging. Part 3. Longshore shoreline boundary conditions for wave-averaged nearshore circulation models", *J. Fluid Mech*., **573**, 399-415.

Baba, Y. and Camenen, B. (2008), "Importance of the swash longshore sediment transport in morphodynamic models", *Proceedings of the Coastal Sediments '07, ASCE*, New Orleans, Louisiana, USA.

Bakhtyar, R., Barry, D.A., Li, L., Jeng, D.S. and Yeganeh-Bakhtiary, A. (2009a), "Modeling sediment transport in the swash zone: A review", *Ocean Eng*., **36**(9-10), 767-783.

Bakhtyar, R., Yeganeh-Bakhtiary, A., Barry, D.A. and Ghaheri, A. (2009b), "Two-phase hydrodynamic and sediment transport modeling of wave-generated sheet flow", *Adv. Water Resour*., **32**(8), 1267-1283.

Bakhtyar, R., Ghaheri, A., Yeganeh-Bakhtiary, A. and Barry, D.A. (2009c), "Process-based model for nearshore hydrodynamics, sediment transport and morphological evolution in the surf and swash zones", *Appl. Ocean Res*., **31**(1), 44-56.

Bakhtyar, R., Barry, D.A., Yeganeh-Bakhtiary, A. and Ghaheri, A. (2009d), "Numerical simulation of surf-swash zone motions and turbulent flow", *Adv. Water Resour*., **32**(2), 250-263.

Bakhtyar, R., Yeganeh-Bakhtiary, A, Barry, D.A. and Ghaheri, A. (2009e), "Euler–Euler coupled two-phase flow modeling of sheet flow sediment motion in nearshore", *J. Coastal. Res*., **56**, 467-471.

Bakhtyar, R., Barry, D.A., Yeganeh-Bakhtiary, A., Li, L., Parlange, J.Y. and Sander, G.C. (2010a), "Numerical simulation of two-phase flow for sediment transport in the inner surf and swash zones", *Adv. Water Resour*., **33**(3), 277-290.

Bakhtyar, R., Razmi, A.M., Barry, D.A., Yeganeh-Bakhtiary, A. and Zou, Q.P. (2010b), "Air-water two-phase flow model of turbulent surf and swash zone wave motions", *Adv. Water Resour*., **33**(12), 1560-1574.

Bakhtyar, R., Brovelli, A., Barry, D.A. and Li, L. (2011), "Wave-induced watertable fluctuations, sediment transport and beach profile change: Modeling and comparison with large-scale laboratory experiments", *Coast. Eng. J*., **58**(1), 103-118.

Bakhtyar, R., Barry, D.A. and Brovelli, A. (2012a), "Numerical experiments on interactions between wave motion and variable-density coastal aquifers", *Coast. Eng. J*., **60**, 95-108.

Bakhtyar, R., Barry, D.A. and Kees, C.E. (2012b), "Numerical experiments on breaking waves on contrasting beaches using a two-phase flow approach", *Adv. Water Resour*., **48**, 68-78.

Bakhtyar, R., Brovelli, A., Barry, D.A., Robinson, C. and Li, L. (2013a), "Transport of variable-density solute plumes in beach aquifers in response to oceanic forcing", *Adv. Water Resour*., **53**, 208-224.

Bakhtyar, R., Dastgheib, A., Roelvink, D. and Barry, D.A. (2016), "Impacts of wave and tidal forcing on 3D nearshore processes in natural beaches. Part I: Flow and turbulence fields", *Ocean Syst. Eng*., In Press [part I].

Bakhtyar, R., Razmi, A. Barry, D.A., Kees, C.E., Yeganeh-Bakhtiary, A. and Miller, C.T. (2013c), "Two-phase flow modeling of the influence of wave shapes and bed slope on nearshore hydrodynamics", *J. Coastal. Res*., **65**, 159-164.

Bayram, A., Larson, M. and Hanson, H. (2007), "A new formula for the total longshore sediment transport rate", *Coast. Eng. J*., **54**(9), 700-710.

Cartier, A. and Héquette, A. (2011a), "Variation in longshore sediment transport under low to moderate conditions on barred macrotidal beaches", *J. Coastal. Res*., **64**, 45-49.

Cartier, A. and Hequette, A. (2011b), "Estimation of longshore and cross-shore sediment transport on sandy macrotidal beaches of northern France", *Proceedings of the Coastal Sediments '11, Miami*, Florida, USA, 2-6 May.

Celikoglua, Y., Yuksel, Y. and Kabdaslı, M.S. (2004), "Longshore sorting on a beach under wave action", *Ocean Eng*., **31**(11-12), 1351-1375.

Chen, Q., Kirby, J.T., Dalrymple, R.A., Shi, F. and Thornton, E.B. (2003), "Boussinesq modeling of longshore currents", *J. Geophys. Res*., **108**, 3362, doi:10.1029/2002JC001308, 2003.

Christensen, E.D., Walstra, D.J. and Emarat, N. (2002), "Vertical variation of the flow across the surf zone", *J. Coast. Eng*., **45**(3-4), 169-198.

Dail, H.J., Merrifield, M.A. and Bevis, M. (2000), "Steep beach morphology changes due to energetic wave forcing", *Mar. Geol*., **162**(2-4), 443-458.

Dastgheib, A., Roelvink, J.A. and Wang, Z.B. (2008), "Long-term process-based morphological modeling of the Marsdiep tidal basin", *Mar. Geol*., **256**(1-4), 90-100.

Dastgheib, A., Roelvink, J.A. and Van der Wegen, M. (2009), "Effect of different sediment mixtures on the long term morphological simulation of tidal basins", *Proceedings of the RCEM* (Santa Fe, Argentina).

Davidson, M.A., Russell, P.E., Huntley, D.A. and Hardisty, J. (1993), "Tidal asymmetry in suspended sand transport on a macrotidal intermediate beach", *Mar. Geol*., **110**(3-4), 333-353.

Delft3D-Flow User Manual 2009. Version: 3.15, Revision: 17474, http://delftsoftware.wldelft.nl/index.php?option=com_docman&task=cat_view&gid=39&Itemid=61, last accessed 2 Feb 2016.

Drake, T.G. and Calantoni, J. (2001), "Discrete particle model for sheet flow sediment transport in the nearshore", *J. Geophys. Res*., **106**, 859-868.

Ellis, J. and Stone, G.W. (2006), "Numerical simulation of net longshore sediment transport and granulometry of surficial sediments along Chandeleur Island, Louisiana, USA", *Mar. Geol*., **232**(3-4), 115-129.

Elfrink, B. and Baldock, T.E. (2002), "Hydrodynamics and sediment transport in the swash zone: A review and perspectives", *Coast. Eng. J*., **45**(3-4), 149-167.

Esteves, L.S., Williams, J.J. and Lisniowski, M.A. (2009), "Measuring and modelling longshore sediment transport", *Coast. Shelf Sci*., **83**(1), 47-59.

Feddersen, F., Guza, R.T., Elgar, S. and Herbers, T.H.C. (1998), "Alongshore momentum balances in the nearshore", *J. Geophys. Res*., **103**, 667-15,676.

Ferguson, R.I. and Church, M. (2004), "A simple universal equation for grain settling velocity", *J. Sediment. Geol*., **74**, 933-937.

Garcez Faria, A.F., Thornton, E.B., Stanton, T.P., Soares, C.V. and Lippmann, T.C. (1998), "Vertical profiles of longshore currents and related bed stress and bottom roughness", *J. Geophys. Res*., **103**, 3217-3232.

Garnier, R., Calvete, D., Falqués, A. and Dodd, N. (2008), "Modelling the formation and the long-term behavior of rip channel systems from the deformation of a longshore bar", *J. Geophys. Res*., **113**(7), C07053, doi:10.1029/2007JC004632.

Hanson, H., Aarninkhof, S., Capobianco, M., Jiménez, J.A., Larson, M., Nicholls, R.J., Plant, N.G., Southgate, H.N., Steetzel, H.J., Stive, M.J.F. and de Vriend, H.J. (2003), "Modelling of coastal evolution on yearly and decadal time scales", *J. Coastal. Res*., **19**(4), 790-811, http://www.jstor.org/stable/4299221, last accessed 1 October 2015

Harcourt-Baldwin, J.L. and Diedericks, G.P.J. (2006), "Numerical modelling and analysis of temperature controlled density currents in Tomales Bay, California", *Estuar. Coast. Shelf Sci*., **66**(3-4), 417-428.

Horn, D.P. and Mason, T. (1994), "Swash zone sediment transport modes", *Mar. Geol*., **120**(3-4), 309-325.

Hughes, S.A. and Chio, T.S. (1981), *Beach and dune erosion during severe storms. Coastal and Oceanographic Engineering Department*, University of Florida, USA. Report No. UFL/COEL/TR/043.

Johnson, B.D. and Smith, J.M. (2005), "Longshore current forcing by irregular waves", *J. Geophys. Res*., **110**(6), C06006, doi:10.1029/2004JC002336.

Kamphuis, J.W. (1991), "Alongshore sediment transport rate", *J. Waterw. Port C. - ASCE.*, **117**(6), 624-641.
Karambas, T.V. (2006), "Prediction of sediment transport in the swash zone by using a nonlinear wave model", *Cont. Shelf Res*., **26**(5), 599-609.
Karunarathna, H., Chadwick, A. and Lawrence, J. (2005), "Numerical experiments of swash oscillations on steep and gentle beaches", *Coast. Eng. J*., **52**(6), 497-511.
Komar, P.D. and Inman, D.L. (1970), "Longshore sand transport on beaches", *J. Geophys. Res*., **30**, 5514-5527.
Kumar, V.S., Anand, N.M., Chandramohan, P. and Naik, G.N. (2003), "Longshore sediment transport rate – measurement and estimation, central west coast of India", *Coast. Eng. J*., **48**(2), 95-109.
Lee, K.H., Mizutani, N., Hur, D.S. and Kamiya, A. (2007), "The effect of groundwater on topographic changes in a gravel beach", *Ocean Eng*., **34**(3-4), 605-615.
Le Méhauté, B. (1970), "A comparison of fluvial and coastal similitude", *Proceedings of the 12th ICCE*, Washington, USA.
Lemos, C.M. (1992), "A simple numerical technique for turbulent flows with free surfaces", *Int. J. Numer. Meth. Fl.*, **15**(2), 127-146.
Lesser, G.R., Roelvink, J.A., van Kester, J.A.T.M. and Stelling, G.S. (2004), "Development and validation of a three-dimensional model", *Coast. Eng. J*., **51**(8-9), 883-915.
Liang, B., Li, H. and Lee, D. (2007), "Numerical study of three-dimensional suspended sediment transport in waves and currents", *Ocean Eng*., **34**(11-12), 1569-1583.
Longuet-Higgins, M.S. (1970), "Longshore currents generated by obliquely incident sea waves", *J. Geophys. Res*., **75**, 6778-6789.
Masselink, G. and Puleo, J.A. (2006), "Swash-zone morphodynamics", *Cont. Shelf Res*., **26**(5), 661-680.
Masselink, G. and Black, K.P. (1995), "Magnitude and cross-shore distribution of bed return flow measured on natural beaches", *Coast. Eng. J*., **25**(3-4), 165-190.
Miles, J., Butt, T. and Russell, P. (2006), "Swash zone sediment dynamics: A comparison of a dissipative and an intermediate beach", *Mar. Geol*., **231**(1-4), 181-200.
Morelissen, R., Bijlsm, A.C. and Tapley, M.J. (2010), "A dedicated tidal stream atlas of the stratified tidal flows near Stonecutters Bridge, Hong Kong, based on 3D numerical simulations with HLES", *J. Hydro-environm. Res*., **3**(4), 224-231.
Newberger, P.A. and Allen, J.S. (2007a), "Forcing a three-dimensional, hydrostatic, primitive-equation model for application in the surf zone: 1. Formulation", *J. Geophys. Res*., **112**, C08018, doi:10.1029/2006JC003472.
Newberger, P.A. and Allen, J.S. (2007b), "Forcing a three-dimensional, hydrostatic, primitive-equation model for application in the surf zone: 2. Application to DUCK94", *J. Geophys. Res*., **112**, C08019, doi:10.1029/2006JC003474.
Pattiaratchi, C.B. and Collins, M.B. (1984), "Sediment transport under waves and tidal currents: A case study from the northern Bristol Channel, U.K.", *Mar. Geol*., **56**(1-4), 27-40.
Pedrozo-Acuna, A., Simmonds, D.J., Chadwick, A.J. and Silva, R. (2007), "A numerical-empirical approach for evaluating morphodynamic processes on gravel and mixed sand-gravel beaches", *Mar. Geol*., **241**(1-4), 1-18.
Polome, P., Marzetti, S. and van der Veen, A. (2005), "Economic and social demands for coastal protection", *Coast. Eng. J*., **52**(10-11), 819-840.
Razmi, A.M., Bakhtyar, R. and Barry, D.A. (2011), "Numerical simulation of two-phase flow for nearshore hydrodynamics under wave-current interactions", *J. Coastal. Res*., **I64**, 1165-1169.
Reeve, D.E. and Fleming, C.A. (1997), "A statistical-dynamical method for predicting long term coastal evolution", *Coast. Eng. J*., **30**(3-4), 259-280.
Reniers, A.J.H.M., Thornton, E.B. and Roelvink, J.A. (2004), "Morphodynamic modeling of an embayed beach under wave-group forcing", *J. Geophys. Res*., **109**(1), C01030, doi:10.1029/2002JC001586.
Reniers, A.J.H.M., MacMagan, J.H., Thornton, E.B., Stanton, T.P., Henriquez, M., Brown, J.W., Brown, J.A. and Gallagher, E. (2009), "Surf zone surface retention on a rip channeled beach", *J. Geophys. Res*., **114**, C10010, doi:10.1029/2008JC005153.

Roelvink, D., Reniers, A., van Dongeren, A., de Vries, J.T., McCall, R. and Lescinski, J. (2009), "Modelling storm impacts on beaches, dunes and barrier islands", *Coast. Eng. J*., **56**(11-12), 1133-1152.

Roelvink, J.A. and Reniers, A.J.H.M. (2012), "A guide to modelling coastal morphology", *Adv. Coast. Ocean Eng*., **12**, World Scientific Publications, Singapore.

Ruggieroa, P., Buijsma, M., Kaminskyc, G.M. and Gelfenbaum, G. (2010), "Modeling the effects of wave climate and sediment supply variability on large-scale shoreline change", *Mar. Geol*., **273**(1-4), 127-140.

Saravanan, S. and Chandrasekar, N. (2010), "Monthly and seasonal variation in beach profile along the coast of Tiruchendur and Kanyakumari, Tamilnadu, India", *J. Iber. Geol*., **36**(1), 39-54.

Trim, L., She, K. and Pope, D.J. (2002), "Tidal effects on cross-shore sediment transport on a shingle beach", *J. Coastal. Res*., **36**, 708-715.

USACE (1984), Shore Protection Manual. Department of the Army, U.S. Corps of Engineers, Washington, DC, USA.

van Rijn, L.C. (2011), *Principles of Sediment Transport in Rivers*, Estuaries and Coastal Seas. AQUA Publications, Amsterdam, The Netherlands.

van Rijn, L.C., Tonnon, P.K. and Walstra, D.J.R. (2011), "Numerical modelling of erosion and accretion of plane sloping beaches at different scales", *Coast. Eng. J*., **58**(7), 637-655.

van Wellen, E., Baldock, T., Chadwick, A.J. and Simmonds, D. (2000), "STRAND: A model for longshore sediment transport in the swash zone", *Proceedings of the 27th International Conference on Coastal Engineering*, ASCE, Sydney, Australia.

van der Wegen, M., Dastgheib, A., Jaffe, B.E. and Roelvink, J.A. (2011), "Bed composition generation for morphodynamic modeling: case study of San Pablo Bay in California, USA", *Ocean Dyn*., **61**(2),173-186.

Warner, J.C., Sherwood, C.R., Signell, R.P., Harris, C.K. and Arango, H.G. (2008), "Development of a three-dimensional, regional, coupled wave, current, and sediment-transport model", *Comput. Geosci*., **34**(10), 1243-1260.

Xin, P., Robinson, C., Li, L., Barry, D.A. and Bakhtyar, R. (2010), "Effects of wave forcing on a subterranean estuary", *Water Resour. Res*., **46**(12), W12505, doi:10.1029/2010WR009632.

Yates, M.L., Guza, R.T., O'Reilly, W.C., Hansen, J.E. and Barnard, P.L. (2011), "Equilibrium shoreline response of a high wave energy beach", *J. Geophys. Res*., **116**(4), C04014, doi:10.1029/2010JC006681.

Abbreviations

ATM	Algebraic turbulence model
H-LES	Horizontal Large Eddy Simulation
LST	Longshore Sediment Transport
NS	Navier-Stokes
SWL	Still Water Level
TKE	Turbulent Kinetic Energy
TDR	Turbulence Dissipation Rate

Nomenclature

Variable	*Description*	*Dimensions*
A	tidal amplitude	L
c	sediment concentration	-
C	Chezy coefficient	$L^{1/2}T^{-1}$
C_D	drag coefficient due to currents	-
D	sediment diameter	L
f_{SUSW}	user-defined tuning parameter	-
h	total water depth	L
$\vec{g}$	gravitational acceleration	LT^{-2}
H	wave height	L
k	turbulent kinetic energy	L^2T^{-2}
M	sediment mobility number due to waves and currents	-
R	submerged specific gravity	-
S_T, S_b, S_S	total, bed load and suspended sediment transport	ML^{-3}
t	time	T
T	wave period	T
U, V	depth-averaged velocity in the horizontal, and curvilinear co-ordinates, respectively	LT^{-1}

U_A	velocity asymmetry value	LT^{-1}
w_s	sediment settling velocity	LT^{-1}

Greek

β	local beach slope	-
μ	dynamic viscosity	$ML^{-1}T^{-1}$
ν	kinematic viscosity	L^2T^{-1}
ν_V	vertical eddy viscosity	L^2T^{-1}
ε	turbulence dissipation rate	L^2T^{-3}
ε_d	eddy diffusivity of sediment	L^2T^{-1}
ρ_f , ρ_s	fluid and sediment densities, respectively	ML^{-3}
ζ	water level above reference (datum)	L
γ	phase lag coefficient	-